

Classical Cepheid Pulsation Models. III. The Predictable Scenario.

Giuseppe Bono¹, Vittorio Castellani², and Marcella Marconi³

ABSTRACT

Within the current uncertainties in the treatment of the coupling between pulsation and convection, the limiting amplitude, nonlinear, convective models appear the only viable approach for providing theoretical predictions about the intrinsic properties of radial pulsators. In this paper we present the results of a comprehensive set of Cepheid models computed within such theoretical framework for selected assumptions on their original chemical composition.

We first discuss the location of the instability strip in the HR diagram, showing that nonlinear predictions on the effective temperature of the instability boundaries substantially differ from similar predictions available in the literature. This discrepancy is mainly due to the nonlinear effects introduced by the interaction between radial and convective motions and to the different physical assumptions adopted for constructing pulsation models. We found that both the blue (hot) and the red (cool) boundaries of fundamental pulsators appear, for each given metallicity, fairly independent of the adopted mass-luminosity relation. As a consequence, it turns out that they can be approximated over a wide luminosity range by a logarithmic relation between stellar luminosity and effective temperature.

We discuss the occurrence of first overtone pulsators and provide an analytical relation for the effective temperature of the predicted blue boundary in metal-poor structures. We also found that predicted fundamental periods based on different assumptions about the mass-luminosity relation can be all nicely fitted, for each given metallicity, by a logarithmic relation which connects the period of the pulsator to mass, luminosity and effective temperature.

¹Osservatorio Astronomico di Roma, Via Frascati 33, 00040 Monte Porzio Catone, Italy; bono@coma.mporzio.astro.it

²Dipartimento di Fisica, Univ. di Pisa, Piazza Torricelli 2, 56100 Pisa, Italy; vittorio@astr18pi.difi.unipi.it

³Osservatorio Astronomico di Capodimonte, Via Moiariello 16, 80131 Napoli, Italy; marcella@na.astro.it

Theoretical predictions concerning pulsation amplitudes in luminosity, radius, velocity, gravity, and effective temperature are discussed and then compared with data available in the current literature. Even though these observables are affected by non negligible observational uncertainties, the agreement between theory and observations is rather satisfactory. Finally, we found that the predicted ratio of the amplitudes in the I and in the V bands appears in very good agreement with the empirical value ($A_I/A_V = 0.6$), with a mild dependence on metallicity.

Subject headings: galaxies: stellar content – stars: distances – stars: evolution – stars: oscillations – stars: variables: Cepheids

1. INTRODUCTION

This is the third paper of a series devoted to the pulsational properties of classical Cepheids predicted by nonlinear pulsation models. In paper I (Bono, Marconi & Stellingwerf 1999) we presented both numerical and physical assumptions adopted for constructing nonlinear, convective models, and discussed the approach to limit cycle stability of both fundamental and first overtone pulsators. By adopting the periods and the modal stability predicted by these models, paper II (Bono et al. 1999a) was focused on the Period-Luminosity (PL), the Period-Color (PC), and on the Period-Luminosity-Color (PLC) relations at selected stellar chemical compositions. Moreover, Bono, Caputo, & Marconi (1998) have already discussed the satisfactory agreement between empirical Cepheid radii and the corresponding theoretical predictions based on this new theoretical scenario.

However, nonlinear models do provide many more predictions, such as the pulsational amplitudes and the morphology of both light and velocity curves, which can be directly compared with the observed Cepheid properties. Even though some of these properties were already investigated on the basis of linear (Chiosi, Wood, & Capitanio 1993; Simon & Young 1997; Saio & Gautschy 1998; Alibert et al. 1999) and nonlinear (Carson & Stothers 1988; Moskalik, Buchler, & Marom 1992) envelope models, several empirical evidence such as the change of luminosity and velocity amplitudes across the instability strip (Sandage & Tammann 1971; Pel 1978; Cogan 1980; Fernie 1990) or the constant amplitude ratio in different photometric bands (Freedman 1988; Tanvir 1997) have not been enlightened by theoretical insights yet. In this paper we supply a comprehensive analysis of pulsation predictions to stimulate further investigations by others working in this field and to discuss the comparison between these theoretical predictions and observational data available in the current literature.

In section 2 we discuss the instability boundaries, we compare them with previous results and discuss the dependence of the boundaries on the adopted chemical composition as well as on the assumptions about the mass-luminosity (ML) relation. In Section 3 we supply suitable analytical relations for fundamental and first overtone pulsators connecting the period to stellar masses, luminosities and effective temperatures. Luminosity, radius, gravity, temperature, and radial velocity amplitudes for fundamental pulsators are discussed in section 4, while first overtone pulsation amplitudes are outlined in section 5. In these two sections we also compare theoretical observables with both photometric and spectroscopic measurements available in the literature. Finally, the main findings of this investigation are summarized in §6, together with some hints on future developments of the present theoretical framework.

Appendix A gives input parameters and theoretical observables for all the computed

pulsation models, while Appendix B presents their predicted light and velocity curves together with a brief discussion on the variation of the morphology across the instability strip.

2. Modal instability and periods

Limiting amplitude, nonlinear, convective models represent a necessary and sufficient condition to assess the modal stability and, in turn, to evaluate the edges of the instability strip for each given stellar structure. In the case of Cepheid variables, one is dealing with intermediate-mass stars which cross the instability region at different luminosities which depend on stellar mass and on chemical composition. The pulsational investigation thus requires suitable assumptions about the ML relation for constraining the predicted luminosity of the model for each given value of the stellar mass. For this purpose we adopted evolutionary predictions presented by Castellani, Chieffi & Straniero (1992, hereinafter CCS92), which were computed for suitable ranges of stellar masses and chemical compositions and under the canonical assumption of no convective core overshooting. Figure 1 shows the comparison between the ML relation adopted in our computations and the relations adopted in linear investigations by Chiosi et al. (1993, hereinafter CWC93) and by Alibert et al. (1999, hereinafter ABHA99). Data plotted in the top panel for $Z=0.02$ show that the quoted evolutionary models are in excellent agreement. As we will discuss later on, a maximum difference of the order of $\Delta \log L \approx 0.1$ has indeed negligible effects on the derived pulsational scenario. The same figure in the bottom panel shows the dependence of the ML relation on the adopted chemical composition. Note that our models assume $Y=0.28$ for $Z=0.02$ and $\Delta Y/\Delta Z=2.5$ for other metallicities, in close similarity with the assumptions made by the quoted authors. In particular, CWC93 adopted $Y=0.25$, $Z=0.004$; $Y=0.25$, $Z=0.008$; and $Y=0.30$, $Z=0.016$, while ABHA99 adopted $Y=0.25$, $Z=0.004$; $Y=0.25$, $Z=0.01$; and $Y=0.28$, $Z=0.02$. Once again we find a rather satisfactory agreement between the different predictions, with a slight enhanced dependence of ABHA99 relations, to be possibly ascribed to different input physics adopted in ABHA99 evolutionary models. However, data plotted in Figure 1 clearly show that we are facing a rather well-established evolutionary scenario.

On the basis of the adopted ML relation we explored the pulsation stability of models at 5, 7, 9, and 11 M_{\odot} with the effective temperature T_e as a free parameter to be moved by steps of 100 degrees across the HR diagram. With this procedure the location of the instability boundaries was evaluated with an accuracy of ± 50 K. The input physics used for constructing both linear and nonlinear envelope models was already described in

paper I and in paper II as well as in Bono et al. (1998). Here we only mention that we adopted OPAL opacities (Iglesias & Rogers 1996) for temperatures greater than 10^4 K, and Alexander & Ferguson (1994) molecular opacities for lower temperatures. In addition an independent set of models was computed for the same values of stellar masses but by increasing the predicted luminosities by $\Delta \log L/L_\odot = 0.25$. According to CWC93, this luminosity shift allows us to explore an evolutionary scenario which accounts for a mild convective core overshooting and therefore to investigate the effects of the mass/luminosity ratio on the pulsation instability. Input parameters and theoretical results for all models characterized by a stable nonlinear limit cycle in the fundamental and/or in the first overtone are presented in Appendix A, Tables 1-4.

Results concerning the fundamental edges of the instability strip are shown in Figure 2 for the two assumed ML relations and the three different stellar metallicities. Data in this figure give the plain evidence that the instability edges depend mainly on luminosity. Noncanonical models -i.e. pulsation models constructed by adopting a ML relation based on mild overshooting evolutionary models- suggest that the red edges at the highest luminosities present a sudden shift toward hotter effective temperatures, with a sharp decrease in the width of the instability strip. We find that both canonical and noncanonical boundaries can be described over a quite large luminosity range by analytical relations of the type $\log T_e = \alpha + \beta \times \log L/L_\odot$. The analytic fits for the red edges were derived by neglecting the noncanonical point at $M = 11M_\odot$, while the blue edge relation for $Z=0.004$ was derived by neglecting the canonical point at $M = 5M_\odot$. Coefficients and errors of both blue and red edge relations for the three different chemical compositions are given in Table 5.

Moreover, data displayed in Figure 2 strongly support the empirical evidence originally pointed out by Pel & Lub (1978) and by Fernie (1990) that Galactic Cepheids present a "wedge-shaped" and not a "rectangular-shaped" instability strip. A similar behavior for Magellanic Cepheids was originally brought out by Martin, Warren, & Feast (1979) and more recently by Caldwell & Laney (1991). This suggests that the narrowing at the lower luminosities is an intrinsic feature of the fundamental instability strip which does not depend on metallicity. Figure 2 shows the additional evidence that at each given luminosity an increase in the metal content shifts the instability strip toward cooler effective temperatures. The dependence of PL, PC, and PLC relations on this effect was thoroughly described in paper II and therefore it is not discussed further.

Figure 3 shows the comparison between our fundamental edges and similar predictions obtained by CWC93 and by ABHA99 from linear, nonadiabatic, convective models. We find that at the lowest metallicity our predicted blue boundaries are located between the two

linear ones, with a slope which appears in good agreement with both CWC93 and ABHA99 results. However, linear red edges appear much steeper than is predicted by nonlinear models. Such a discrepancy is not surprising, since the linear approach does not account for the coupling between pulsation and convection, and therefore can hardly predict the modal stability of models located close to the cool edge. To cope with such a difficulty, linear red edge estimates by CWC93 and by ABHA99 were not fixed at the effective temperature where the fundamental growth rate attains vanishing values but, more or less tentatively, at the effective temperature where the growth rate attains its maximum value (Chiosi et al. 1992; ABHA99). Present nonlinear results suggest that such an assumption is far from being adequate, a conclusion further supported by the evidence that ABHA99 predictions fail to reproduce the already discussed empirical evidence for a "wedge-shaped" instability strip. The difference in the blue edges provided by CWC93 and ABHA99 also suggests that linear predictions depend on the numerical and physical assumptions adopted for constructing pulsation models.

Moreover, one may notice that an increase in the metal content causes a flattening in the slope of the nonlinear blue boundary, at variance with the predicted linear behavior. Such an occurrence is probably connected with the evidence that a metallicity increase shifts the blue edge toward cooler effective temperatures. As a consequence, metal-rich models show a stronger dependence on the nonlinear effects introduced by the coupling between pulsation and convection than metal-poor ones. The reader interested in a detailed discussion on the dependence of modal stability and pulsation properties on these effects is referred to paper I.

Figure 4 shows the location in the HR diagram of first overtone unstable models we found for the three selected chemical compositions in the lower portion of the explored luminosity range. In this region for the two lower metallicities we derived the following linear analytical relations for first overtone blue boundaries:

$$\log T_e^B(Z = 0.004) = -0.047(\pm 0.005) \log L + 3.954(\pm 0.002) \quad \sigma = 0.002$$

$$\log T_e^B(Z = 0.008) = -0.067(\pm 0.004) \log L + 4.011(\pm 0.001) \quad \sigma = 0.001$$

where L is the luminosity (solar units), T_e is the effective temperature (K), and σ is the standard deviation.

3. Pulsation relations

During the last few years several authors (CWC93; Simon & Young 1997; Saio & Gautschy 1998) have used linear, nonadiabatic models to derive pulsational relation connecting periods to stellar masses and luminosities. In paper I (see Fig. 53) we already compared theoretical periods based on both linear and nonlinear models. We found that nonlinear periods of high-mass Cepheids are from 1% to 10% shorter than the linear ones when moving from the blue to the red edge of the instability strip. This difference can introduce an uncertainty of the order of 0.08 mag in the comparison between theoretical and empirical PL relations. This finding supports the relevance of precise pulsation relations.

Fortunately enough, we find that at each given chemical composition the present nonlinear values of canonical and noncanonical fundamental periods follow with very good accuracy a linear relation connecting $\log P$ to the logarithms of the pulsator mass, luminosity, and effective temperature. The coefficients and the errors of these analytical relations are given in Table 6. Figure 5 shows how accurately these relations fit the periods of the computed models. It is now possible to estimate the effects of uncertainties in the adopted ML relation. Going back to Figure 1 we find that at fixed luminosity -the physical parameter governing the instability boundaries- current canonical ML relations predict quite similar mass values. In fact, the difference at $\log L/L_{\odot} = 3.5$ between CCS92 and CWC93 is $\delta \log M \approx \pm 0.01$, while between CCS92 and ABHA99 is $\delta \log M \approx \pm 0.02$. This difference causes a period uncertainty of 2% and 4% respectively and, in turn, of only few hundreds of magnitude on the distances obtained by adopting the theoretical PL relation. On the other hand, the mass difference between canonical and noncanonical ML relations is of the order of $\delta \log M \approx \pm 0.07$ which implies a 14% period uncertainty and, in turn, an uncertainty of about 0.15 mag on the distance modulus. However, this uncertainty affects absolute but not relative distance determinations due to the systematic difference between the two different evolutionary frameworks over the whole period range.

Data in Figure 5 shows that for each given effective temperature an increase in metallicity, in spite of the decrease in luminosity, causes a small increase in the pulsation period of the order of 0.03 dex when moving from $Z=0.004$ to $Z=0.02$. However, an increase in metallicity has the major effect of shifting the instability strip toward lower effective temperatures and therefore longer periods. As already discussed in Paper II, such a shift plays a key role in governing the dependence of the PL relation on metallicity. This shift in temperature also provides a plain explanation of the empirical evidence originally pointed out by Gascoigne (1969, 1974) and more recently by Sasselov et al. (1997) that Cepheids in the Small Magellanic Cloud (SMC) are, for a given period, bluer than Cepheids in the LMC. Alternatively, we predict that at fixed luminosity the period distribution of SMC

Cepheids should be shifted toward shorter periods when compared with LMC Cepheids. The cumulative period distributions of Cepheids in LMC and in SMC recently derived by the EROS project suggest a similar trend (Marquette 1998), but we still lack a detailed comparison between the period distribution of both LMC and SMC Cepheids at fixed magnitude bins.

In the explored range of luminosities we found a relatively small number of first overtone pulsators. This mode is indeed unstable only in low-mass ($5 - 7M_{\odot}$) and therefore low-luminosity models. Owing to the mild dependence of first overtone periods on metallicity we derived a single pulsational relation which does not account for the metallicity dependence:

$$\log P = 10.763(\pm 0.002) + 0.672(\pm 0.002)\log L - 3.305(\pm 0.039)\log T_e \quad \sigma = 0.002$$

where symbols have their usual meaning.

4. Pulsational amplitudes: fundamental pulsators

4.1. Luminosity

Dating back to the seminal investigation by Sandage & Tammann (1971, hereinafter ST71), the luminosity amplitude has been recognized as a key parameter for assessing the pulsation properties of classical Cepheids. If amplitudes, as suggested by the quoted authors (see also Sandage 1972), depend on the distance from the edges of the instability strip, this parameter could be used to properly locate a Cepheid within the strip, and in turn to use a Period-Luminosity-Amplitude relation for estimating distances. However, empirical evidence concerning the behavior of the luminosity amplitude inside the strip, the so-called "amplitude mapping", turned out to be quite controversial. On the basis of Cepheid samples in four different galaxies, ST71 suggested that in the period range from $\log P \approx 0.40$ to 0.86 and for $\log P > 1.3$ the largest luminosity amplitudes are attained close to the blue edge, while the trend is reversed for Cepheids with periods ranging from $\log P = 0.86$ to $\log P = 1.3$. A similar conclusion for Galactic Cepheids was reached by Cogan (1980), who suggested to move the cut-off period from $\log P = 1.3$ to 1.1 .

On the other hand, Madore (1976) suggested, on the basis of empirical relations provided by Fernie (1970), that classical Cepheids attain the largest amplitudes close to the red edge, whereas Butler (1976,1978) found an opposite trend among MC Cepheids. More recently Fernie (1990) investigated a large sample of Galactic Cepheids suggesting that for a given period the largest amplitudes are possibly attained close to the center of the

instability strip, even though they are not tightly correlated with the position in the strip.

Figure 6 shows bolometric amplitudes of both canonical and noncanonical models as a function of period for the various given masses and for the three selected metallicities. In this figure each sequence of models depicts the predicted amplitudes across the instability strip. A glance at the data plotted in Figure 6 discloses that for the three explored metallicities the pulsators in the short-period range (i.e. with lower masses and luminosities) attain their maximum amplitude at the blue edge, whereas toward longer periods the amplitudes present a "bell-shaped" distribution.

Such a behavior is similar to the trend found in fundamental RR Lyrae pulsators (Bono et al. 1997, hereinafter BCCM97): at the luminosities where the fundamental blue boundary falls in a region where the first overtone is already unstable, the amplitude of fundamental pulsators steadily decreases from the blue to the red edge, whereas at the luminosities in which only the fundamental pulsators attain a stable nonlinear limit cycle the pulsation amplitudes show a "bell-shaped" variation from the hot to the cool edge of the instability strip. However, we notice that in the large majority of cases the maximum amplitude is attained only few hundred degrees from the blue boundary, and then the amplitude steadily decreases from the blue to the red over a large portion of the strip. Therefore theoretical results appear in reasonable agreement with the empirical evidence brought out by ST71 and by Cogan (1980).

Another feature disclosed by data plotted in Figure 6 is that an increase in the metal content generally causes a decrease in the maximum amplitudes. This trend supplies a sound support to the empirical evidence originally suggested by Arp & Kraft (1961) and then confirmed by van Genderen (1978) on the basis of a large sample of short-period Galactic and Magellanic Cepheids. The only exceptions to this rule are the $7 M_{\odot}$ (canonical) for $Z=0.02$ and the $9 M_{\odot}$ (noncanonical) models for $Z=0.008$ which show a larger bolometric amplitude when compared with more metal-poor models of the same mass value. This peculiarity could be due to a nonlinear behavior of the thermal properties of the outermost layers caused by the shock propagation close to the phases of maximum amplitude (see paper I). In fact, as we will discuss later on, the radial velocity amplitudes of these models do not show this peculiar behavior.

The sequence of canonical models at $7 M_{\odot}$ presents a "double-peaked" distribution with two maxima located close to the blue and to the red edge. Interestingly enough, these models attain the minimum amplitude at $\log P \approx 1.03$, in remarkable agreement with the minimum at $\log P = 1.05 \pm 0.03$ in the empirical distribution of Fourier parameters ϕ_{21} and R_{21} found in LMC Cepheids by MACHO (Welch et al. 1997) and EROS projects (Beaulieu & Sasselov 1997). The physical mechanism(s) which govern the appearance of

such a phenomenon and the dependence on chemical composition will be discussed in a forthcoming paper (Bono et al. 1999b). Finally we note that the period-amplitude variation of this sequence supports the local minimum in B amplitudes found in this period range by van Genderen (1978) for LMC Cepheids. This finding is very encouraging since the Bailey diagram (luminosity amplitude vs. period) does not depend on distance modulus and on color-temperature relation, and presents a negligible dependence on bolometric correction scale and on reddening.

Figure 7 shows the comparison in the Bailey diagram between pulsation amplitudes in the V band of Galactic Cepheids collected by Fernie et al. (1995) and theoretical predictions for $Z=0.008$ and $Z=0.02$. The choice of metallicities follows the results of a recent spectroscopic investigation by Fry & Carney (1997), which supports the evidence that Galactic calibrating Cepheids cover this metallicity range. Bolometric amplitudes were transformed into V amplitudes by adopting the bolometric corrections provided by Castelli, Gratton, & Kurucz (1997a,b). We assumed $M_{bol}(\odot) = 4.62$. Theoretical V amplitudes show the same variation of bolometric amplitudes across the instability strip and are in satisfactory agreement with empirical values both at short and at long-periods. The only exception are the models at $M = 7M_{\odot}$, $Z=0.02$ and $M = 9M_{\odot}$, $Z=0.008$ whose V amplitudes are 20-25% higher than the observed ones. However, it is noteworthy that the luminosity amplitudes predicted by nonlinear *radiative* models are at least a factor of two larger than those predicted by *convective* ones (see Figure 1 in Bono & Marconi 1998).

The period-amplitude behavior of Galactic Cepheids was extensively investigated by van Genderen (1974) who found that the envelope line of B amplitudes attains a constant value for $0.5 \leq \log P \leq 1.0$ and then a rapid increase up to $\log P = 1.15$. Toward longer periods the envelope line attains once again a constant value up to $\log P = 1.5$ and then a steady decrease (see data plotted in his Figure 1). This empirical evidence was subsequently confirmed by Laney & Stobie (1993) by adopting infrared J, H, and K amplitudes for 51 Galactic Cepheids. Theoretical predictions plotted in Figures 6 and 7 seem to support this behavior, but to confirm this evidence further models at solar chemical composition in the period range $0.7 \leq \log P \leq 1.0$ are needed.

4.2. Amplitude ratio

The agreement between theory and observations on the behavior of the luminosity amplitude inside the instability strip suggested to test the empirical assumption that the amplitude ratio between the I (Cousins) and the V (Jonhson) bands is equal to 0.6 mag (Tanvir 1997). This assumption is generally adopted (Freedman 1988) for deriving

the I-band light curve on the basis of the shape of the V-band light curve and thus for reducing the number of individual measurements necessary for estimating the mean I magnitude. Amplitude ratios in different photometric bands are also interesting because as demonstrated by Coulson & Caldwell (1989) they can be adopted for discovering companions to Cepheids (see also Laney & Stobie 1993).

Figure 8 shows the predicted A_I/A_V ratio as a function of the pulsation period for canonical, fundamental pulsators at the three adopted metallicities. Luminosity amplitudes in the I band were estimated by adopting the color-temperature relations provided by Castelli et al. (1997a,b). Data plotted in this figure show that the mean A_I/A_V ratio ranges from 0.64 ± 0.03 at $Z=0.004$ and $Z=0.008$ to 0.65 ± 0.02 at $Z=0.02$. This result suggests that, within the intrinsic dispersions, the A_I/A_V ratio is in average constant and slightly higher than the empirical value currently adopted. However, this finding mainly depends on stellar atmosphere models, and indeed some numerical experiments performed by artificially enhancing both the surface gravity and the effective temperature variations along the pulsation cycle caused an increase in the A_I/A_V ratio smaller than 10%.

4.3. Radial velocity

Even though radial velocity amplitudes are available only for a limited number of Galactic Cepheids, this observable can supply useful information on the dynamical behavior across the instability strip. Data listed in Tables 2 and 4 show that the behavior of radial velocity curves are largely correlated to the already discussed light curves. The main difference is found in $5M_\odot$ canonical models at $Z=0.004$ and $Z=0.008$, which show very large Δu values when compared with more massive models. Since the bolometric amplitudes do not present this behavior, it turns out that in these models the bolometric amplitude over a full pulsation cycle is governed by temperature variations more than by radius variations.

The top panel of Figure 9 shows the comparison between empirical pulsational velocity amplitudes for Galactic Cepheids provided by Bersier et al. (1994), Bersier & Burki (1996) and by Bersier (1999, private communication) and theoretical predictions for $Z=0.02$ and $Z=0.008$. The bottom panel of Figure 9 shows a similar comparison but with empirical data collected by Cogan (1980). In the Cogan sample we identified Cepheid variables by means of a cross-identification with the database on Galactic Cepheids provided by Fernie et al. (1995) and among them we selected the objects presenting accurate velocity amplitudes. Pulsational velocities plotted in Figure 9 were derived from the empirical radial velocity amplitudes by adopting a projection factor of 1.36, as suggested by Bersier & Burki (1996). However, we notice that in the literature quite different values were suggested, with the

additional evidence that the projection factor could change when moving from short to long-period Cepheids (Gieren et al. 1989) as well as along the pulsation cycle (Sabbey et al. 1995). We adopted this value since its effect is marginal when compared to observational errors affecting non homogeneous spectroscopic measurements plotted in the bottom panel. In fact, we estimated that the difference in the velocity amplitude among objects included both in the Bersier et al. and in the Cogan samples ranges from few percent to more than 20%.

Figure 9 shows that theoretical predictions appear in reasonable agreement with observations over the whole period range. In particular, one may notice that toward longer periods $-\log P = 1.5 \div 1.6$ - the velocity amplitudes decrease to approximately 50 km/sec, in agreement with theoretical predictions. However, from $\log P = 1.1$ to $\log P = 1.5$ our computations predict pulsators with smaller velocity amplitudes that are marginally supported by current empirical estimates. We can hardly assess whether this discrepancy is due to a selection effect or because theoretical amplitudes are too small close to the instability boundaries. Even by accounting for the quoted spread in metallicity the discrepancy between theory and observations is still present. In fact, models at $Z=0.008$ predict both high and small velocity amplitudes in the period range $\log P = 1.1 \div 1.5$.

However, on a very general ground, data plotted in Figure 9 show that limiting amplitude models which include a proper treatment of the pulsation/convection interaction seem to solve the long-standing discrepancy between theoretical and observed velocity amplitudes. In fact, velocity amplitudes across the instability strip predicted by nonlinear radiative models are systematically larger than the observed ones (Carson & Stothers 1988; Moskalik et al. 1992).

4.4. Radius, gravity and temperature

Empirical estimates of radius, gravity and temperature amplitudes are unfortunately rather scanty. In the following we will refer to the last comprehensive investigations on this subject provided by Pel (1978, 1980) and based on a large set of photometric data in the Walraven system. We find that theoretical fractional radius variations $-\Delta R/R_{ph}$ - for $Z=0.02$ and $Z=0.008$ and for periods shorter than 11 d show -in agreement with empirical data- a decrease when moving from the blue to the red edge. However, predicted values appear somehow smaller than the observed ones, since the observed $\Delta R/R_{ph}$ values range from more than 20% close to the blue edge to 5% at the red edge, whereas theoretical predictions range from 10-15% close to the blue edge to 5% at the red edge. The origin of such a discrepancy cannot be firmly established since we lack an estimate of the observational

uncertainties as well as data for long-period Cepheids. Moreover, Pel's results relied on old atmosphere models (Kurucz 1975) which could considerably affect estimation of these parameters.

Theoretical and observed effective gravity amplitudes $-\Delta g_e$ appear in reasonable qualitative agreement. The bulk of the empirical estimates by Pel (1978) for bright Cepheids with $P < 11$ d is around $\Delta g_e \approx 0.4$, and range roughly from 0.22 to 0.9. The theoretical ones attain similar values and range from 0.3 to 0.8. Obviously, spectroscopic investigations can supply tighter constraints on the accuracy of theoretical predictions.

The agreement we found for gravity amplitudes applies also to fractional temperature variations. Empirical estimates by Pel (1978) range approximately from $\Delta\Theta_e=0.06$ to 0.22, while the theoretical ones from $\Delta\Theta_e=0.07$ to 0.18, where $\Theta_e = 5040/T_e$. This qualitative agreement is further supported by recent spectroscopic investigations on the temperature amplitudes in a small sample of Galactic Cepheids collected by Bersier, Burki, & Kurucz (1997). Since the thermal behavior along the pulsation cycle strongly depends on the coupling between pulsation and convection, such qualitative agreement in the short-period range supports, within current observational uncertainties, the treatment adopted to account for the convective transport.

5. Pulsational amplitudes: first overtone pulsators

In Figure 10 from top to bottom are shown bolometric and radial velocity amplitudes, fractional radius and temperature variations for first overtone pulsators. Data plotted in this figure show that in canonical models an increase in the metal content causes a decrease in the pulsation amplitudes (see also paper I). Unfortunately, the small number of unstable first overtone pulsators does not allow us to find out a clear trend concerning the change of the pulsation amplitudes from the blue to the red edge of the instability strip. Canonical, metal-poor models at $5M_\odot$ show a linear decrease in the bolometric amplitude and in the fractional temperature variation, while amplitudes of more metal-rich and noncanonical models present across the instability strip the characteristic "bell-shaped" variation we already found for first overtone RR Lyrae models (BCCM97).

In order to supply a useful theoretical framework for first overtone identification among field stars, the light and velocity curves of all first overtone models are presented in appendix A. Data plotted in Figures 10-21 show that the shape of both light and velocity curves of first overtone models are almost sinusoidal and resemble the empirical light curves for s -Cepheids recently observed by the EROS project in the bar of the LMC (Beaulieu et

al. 1995). However, it is worth noting that the shape of the light curve of canonical models at $M = 5M_{\odot}$ and $Z=0.004$ are not sinusoidal, and indeed the rising branch is steeper than the decreasing branch. Moreover both canonical and noncanonical models located in the middle of the instability strip and with period ranging from $P=1.934$ d to $P=3.811$ d also show a well defined bump just before the luminosity maximum. This feature is also present in models at $Z=0.008$ with periods ranging from $P=2.076$ d to $P=3.816$ d.

Empirical light curve Fourier parameters ϕ_{21} of *s*-Cepheids show a sudden jump close to $P=3.2$ d when plotted as a function of the pulsation period. This abrupt change was explained as a 2 : 1 resonance between the first and the fourth overtone (Antonello & Poretti 1986; Petersen 1989). Current radiative hydrodynamical models fail to reproduce this empirical behavior, and in particular the appearance around the quoted period of the bump along the light curve (Kienzle et al. 1999, and references therein). A detailed analysis of this phenomenon is beyond the scope of this investigation. However, the evidence that the bump along the light curve of first overtone pulsators is located in the right period range suggests that nonlinear, convective models can shed new light on this long-standing problem.

CORAVEL radial velocity amplitudes for Galactic first overtone pulsators have been recently collected by Bersier et al. (1994) and by Kienzle et al. (1999, and references therein). Theoretical predictions appear once again in reasonable agreement with empirical data, since close to $\log P = 0.35$ both data sets attain values of the order of 20-25 km/sec. The same agreement is found for fractional temperature variations, and indeed both empirical and theoretical observables for Galactic Cepheids (Bersier et al. 1997) with period shorter than $\log P = 0.5$ range approximately from $\Delta T_e/T_e=0.05$ to 0.09. However, we do not put forward the comparison between theory and observations since first overtone models need to be extended to lower stellar masses before firm conclusions on the behavior of this mode within the instability strip can be reached.

6. Summary and conclusions

In this paper we presented the large set of pulsational properties predicted by our classical Cepheid, limiting amplitude, nonlinear, convective models constructed by adopting three different assumptions on chemical composition. We first discussed the location of the instability strip in the H-R digram, and showed that the instability edges predicted by nonlinear models are substantially different from the linear ones. This difference is mainly caused by the nonlinear effects of the coupling between pulsation and convection which is not included in linear, nonadiabatic, convective models. For each given metallicity we

find that both blue and red boundaries of fundamental pulsators appear fairly independent of the adopted ML relation, and indeed they can be approximated over a quite large luminosity range by an analytical relation between $\log L$ and $\log T_e$.

The occurrence of first overtone pulsators in the lower mass range is also discussed and the linear analytical relations for the blue boundaries of metal-poor structures $-Z=0.004$, $Z=0.008$ - are provided as well. We also found that predicted fundamental periods, at fixed chemical composition, can be nicely fitted by an analytical relation connecting the logarithmic period to $\log M$, $\log L$ and $\log T_e$ independently of the assumption about the ML relation. These findings supply straightforward theoretical support to the use of Cepheid PL relation for estimating distances, since the topology of the instability strip presents, at fixed chemical composition, a negligible dependence on the ML relation. A similar conclusion, though based on empirical evidence, was reached by Tanvir (1997, and references therein).

Theoretical predictions concerning luminosity, radius, velocity, gravity, and temperature amplitudes are discussed in connection with observational data available in the current literature. As a whole, we found a rather satisfactory agreement, within the present large observational uncertainties, between theory and observations. The exhaustive discussion on theoretical observables presented in this investigation was mainly aimed at stimulating further detailed comparison with spectroscopic and photometric data which can supply tight constraints on the adequacy and consistency of the input physics adopted for constructing nonlinear pulsation models.

We also mention that Cepheids for which estimates of both stellar mass and effective temperature (or color) are available, such as Cepheids in stellar clusters (Bono & Marconi 1997) or in binary systems (Böhm-Vitense et al. 1998, and references therein), can supply useful suggestions on the accuracy of predicted periods, and in turn on the ML relation which governs these objects. In fact, together with Cepheids in LMC and SMC stellar clusters which are a fundamental laboratory for studying their evolutionary and pulsational properties, current empirical estimates suggest that the incidence of binaries among field Cepheids ranges from 30% (Evans 1992) to more than 50% (Szabados & Pont 1998).

We conclude that the nonlinear theoretical framework appears to be the only approach which can supply a reliable description of the pulsation behavior in radial pulsators. Moreover, it turns out that limiting amplitude calculations are a fundamental requirement for estimating on a firm basis both the modal stability and the intrinsic properties to be compared with observed variable stars (see also Ya'ari & Tuchman 1999).

We are particularly grateful to D. Bersier for sending us Cepheid radial velocity data in electronic form and for new data in advance of publication as well as for a detailed reading

of an early draft of this paper. We are also grateful to D. Alves, F. Caputo, D. Laney and N. Panagia for many insightful discussions on Cepheid properties. In addition, we acknowledge an anonymous referee for some useful remarks that served to improve the paper. This work was supported, in part, by the Ministero dell'Università e della Ricerca Scientifica e Tecnologica -Cofinanziamento 98- under the project "Stellar Evolution". Partial support by Agenzia Spaziale Italiana is also acknowledged.

A. Predicted observables

In order to provide a useful theoretical framework which accounts for the systematic properties of Cepheids to be compared with actual properties of observed variables, Tables 1-4 summarize the observables of all limiting amplitude, nonlinear, convective models we computed.

Tables 1 and 2 list both input parameters and pulsational amplitudes for first overtone and fundamental pulsators constructed by adopting a ML relation based on evolutionary models which neglect the convective core overshooting. In particular, columns 1, 2, and 3 report the stellar mass (solar units), the logarithmic luminosity (solar units), and the static effective temperature (K) adopted for each model. From left to right the other quantities listed in these tables are: 4) nonlinear period (d); 5) mean radius (solar units); 6) fractional radius oscillation i.e. $\Delta R/R_{ph} = (R^{max} - R^{min})/R_{ph}$ where R_{ph} is the photospheric radius; 7) radial velocity amplitude (km s^{-1}) i.e. $\Delta u = u^{max} - u^{min}$; 8) bolometric amplitude (mag.) i.e. $\Delta M_{bol} = M_{bol}^{max} - M_{bol}^{min}$; 9) logarithmic amplitude of static gravity i.e. $\Delta \log g_s = \log g_s^{max} - \log g_s^{min}$; 10) logarithmic amplitude of effective gravity i.e. $\Delta \log g_{eff} = \log g_{eff}^{max} - \log g_{eff}^{min}$ where $g_{eff} = GM/R^2 + du/dt$; 11) temperature amplitude (K) i.e. $\Delta T = T^{max} - T^{min}$ where T is the temperature of the outer boundary; 12) effective temperature amplitude (K) i.e. $\Delta T_e = T_e^{max} - T_e^{min}$ where T_e is derived from the surface luminosity. With the exception of the effective gravity, the quantities reported in column 4 to 11 are referred to the surface zone. The mean effective gravity of the outermost layers was estimated by adopting the procedure suggested by Bono, Caputo & Stellingwerf (1994). The temperature amplitudes listed in column 10 and 11 have been rounded to the nearest 50 K. At fixed stellar mass, luminosity level and chemical composition the temperature of the blue (red) edges can be estimated by increasing (decreasing) the effective temperature of the hottest (coolest) unstable model by 50 K.

Tables 3 and 4 report the same quantities of Tables 1 and 2 but refer to envelope models constructed by adopting a ML relation typical of evolutionary models which account for a mild convective core overshooting (see paper I for details).

B. Light and velocity curves

The morphology of both light and velocity curves play a key role for assessing Cepheid pulsation modes and also for constraining the pulsation behavior of these variables across the instability strip. Figures 11-34 show the light (left panel) and velocity (right panel) variations throughout two consecutive cycles. Solid and dashed lines refer to fundamental and first overtone pulsators respectively. Figures 11-22 show the Cepheid sequences constructed by adopting a canonical ML relation, while figures 23-34 the sequences based on a noncanonical one. However, figures 11-14 as well as 23-26 ($M/M_{\odot}=5,7,9,11$; $Y=0.25$; $Z=0.004$) are published in the printed edition, while figures 15-18 and 27-30 ($M/M_{\odot}=5,7,9,11$; $Y=0.25$; $Z=0.008$), together with figures 19-22 and 31-34 ($M/M_{\odot}=5,7,9,11$; $Y=0.28$; $Z=0.02$) are only available in the on-line edition.

The first extensive nonlinear investigations on the shape of theoretical light and velocity curves of Cepheids date back to Christy (1966, 1975 and references therein), Stobie (1969) and more recently to Carson & Stothers (1988) and Moskalik et al. (1992). Light and velocity curves presented in Figures 11-34, when compared with similar predictions available in the literature, do not show spurious features such as spikes and/or ripples throughout the pulsation cycle (see also paper I). In this context it is worth mentioning that Christy (1975) on the basis of leading physical arguments, suggested that the main Cepheid features can be correlated to the *Christy parameter* $P/(R/R_{\odot})$. Even though Christy's predictions were based on nonlinear, radiative, small amplitude models, current convective models support his findings concerning the systematics of Cepheid properties. In fact we found, in agreement with Christy, that the transition from first overtone to fundamental pulsators takes place close to $P/(R/R_{\odot}) \approx 0.1$. Moreover, our models show that the appearance of the bump along the decreasing branch takes place close to $P/(R/R_{\odot}) \approx 0.12$ and falls at earlier pulsation phases when moving toward longer period Cepheids. Christy predicted a similar behavior but for slightly larger $P/(R/R_{\odot})$ values.

Unfortunately our models do not reach very long periods ($P > 130$ d) and therefore we cannot assess on firm basis whether Cepheids in this region of the instability strip are characterized by an irregular behavior and by very large amplitudes. Finally, we mention that our models do not present RV Tauri characteristics, i.e. alternations of deep and shallow minima in both light and velocity curves in the period range 25 – 40 d, as suggested by Moskalik & Buchler (1991) and by Moskalik et al. (1992). Since these calculations were performed by adopting similar ML relations, we suspect that this difference is caused by different assumptions on the energy transport mechanism (radiative versus convective).

REFERENCES

- Alexander, D. R., & Ferguson, J. W. 1994, *ApJ*, 437, 879
- Alibert, Y., Baraffe, I., Hauschildt, P. & Allard, F. 1999, *A&A*, astro-ph/9901294 (ABHA99)
- Antonello, E., & Poretti, E. 1986, *A&A*, 169, 149
- Arp, H. C., & Kraft, R. P. 1961, *ApJ*, 133, 420
- Beaulieu, J. P. et al. 1995, *A&A*, 303, 137
- Beaulieu, J. P. & Sasselov, D. D. 1997, in *Variable Stars and the Astrophysical Returns of Microlensing Surveys*, ed. R. Ferlet, J.P. Maillard & B. Raban, (Editions Frontières: Gif-sur-Yvette Cedex), 193
- Bersier, D., & Burki G. 1996, *A&A*, 306, 417
- Bersier, D., Burki G., & Kurucz, R. L. 1997, *A&A*, 320, 228
- Bersier, D., Burki G., Mayor, M., & Duquenooy, A. 1994, *A&AS*, 108, 25
- Bono, G., Caputo, F., Castellani, V. & Marconi, M. 1997, *A&AS*, 121, 327 (BCCM97)
- Bono, G., Caputo, F., Castellani, V. & Marconi, M. 1999a, *ApJ*, 512, 711 (paper II)
- Bono, G., Caputo, F., & Marconi, M. 1998, *ApJ*, 497, L43
- Bono, G., Caputo, F., & Stellingwerf, R. F. 1994, *ApJ*, 432, 51
- Bono, G., & Marconi, M. 1997, *MNRAS*, 290, 353
- Bono, G., & Marconi, M. 1998, in *A Half Century of Stellar Pulsation Interpretations: a Tribute to A.N. Cox*, ed. P.A. Bradley & J.A. Guzik (San Francisco: ASP), 287
- Bono, G., Marconi, M., & Stellingwerf, R. F. 1999, *ApJS*, 125, in press (paper I)
- Bono, G., et al. 1999b, in preparation
- Böhm-Vitense, E., Evans, N. R., Carpenter, K., Albrow, M. D., Cottrell, P. L., Robinson, R. & Beck-Winchatz, B. 1998, *ApJ*, 505, 903
- Butler, C. J. 1976, *A&AS*, 24, 299
- Butler, C. J. 1978, *A&AS*, 32, 83

- Caldwell, J. A. R., & Laney, C. D. 1991, in IAU Symp. 148, The Magellanic Clouds, ed. R. Haynes & D. Milne (Dordrecht: Kluwer), 249
- Carson, R. T., & Stothers, R. B. 1988, ApJ, 328, 196
- Castellani, V., Chieffi, A. & Straniero, O. 1992, ApJS, 78, 517 (CCS92)
- Castelli, F., Gratton, R. G., & Kurucz, R. L. 1997a, A&A, 318, 841
- Castelli, F., Gratton, R. G., & Kurucz, R. L. 1997b, A&A, 324, 432
- Chiosi, C., Wood, P. R., Bertelli, G., & Bressan, A., 1992, ApJ, 387, 320
- Chiosi, C., Wood, P. R., & Capitanio, N. 1993, ApJS, 86, 541 (CWC93)
- Christy, R. F. 1966, ApJ, 145, 340
- Christy, R. F. 1975, in Cepheid Modeling, eds. D. Fischel, & W.M. Sparks, (Washington: NASA SP-383), 85
- Cogan, B. C. 1980, ApJ, 239, 941
- Coulson, I. M., & Caldwell, J. A. R. 1989, MNRAS, 240, 285
- Evans, N. R. 1992, AJ, 384, 220
- Fernie, J. D. 1970, ApJ, 161, 679
- Fernie, J. D. 1990, ApJ, 354, 295
- Fernie, J. D., Evans, N. R., Beattie, B., & Seager, S. 1995, IBVS, 4148, 1
- Freedman, W. L. 1988, ApJ, 326, 691
- Fry, A. M. & Carney, B. W. 1997, ApJ, 113, 1073
- Gascoigne, S. C. B. 1969, MNRAS, 146, 1
- Gascoigne, S. C. B. 1974, MNRAS, 166, 25
- Gieren, W. P., Barnes, T. G. III, Moffett, T. J. 1989, ApJ, 342, 467
- Iglesias, C. A., & Rogers, F. J. 1996, ApJ, 464, 943
- Kienzle, F., Moskalik, P., Bersier, D. & Pont, F. 1999, A&A, 341, 818

- Kurucz, R. L. 1975, in Multicolor Photometry and the HR diagram, ed. A.G. Davis Philip & D.S. Hayes, Dudley Observatory Reports, 9, 271
- Laney, C. D., & Stobie, R. S. 1993, MNRAS, 260, 408
- Madore, B. F. 1976, Observatory, 96, 245
- Marquette, J. B. 1998, in IAU Symp. 190, New Views of the Magellanic Clouds, ed. Y.-H. Chu, N. Suntzeff, J. Hesser, & D. Bohlender (ASP: San Francisco), in press
- Martin, W. L., Warren, P. R., & Feast, M. W. 1979, 188, 139
- Moskalik, P., & Buchler, R. 1991, ApJ, 366, 300
- Moskalik, P., Buchler, R., & Marom, A. 1992, ApJ, 385, 685
- Pel, J. W. 1978, A&A, 62, 75
- Pel, J. W. 1980, in Current Problems in Stellar Pulsation Instabilities, ed. D. Fischel, J. Rountree Lesh, & W.M. Sparks, (NASA SP-625; Washington, DC: NASA), 1
- Pel, J. W. & Lub, J. 1978, in IAU Symp. 80, The H-R diagram, ed. A.G. Davis Philip & D.S. Hayes, (Dordrecht: Reidel), 229
- Petersen, J. O. 1989, A&A, 226, 151
- Sabbey, C. N., Sasselov, D. D., Fieldus, M. S., Lester, J. B., Venn, K. A., & Butler, R. P. 1995, ApJ, 446, 250
- Saio, H. & Gautschy, A. 1998, ApJ, 1998, 498, 360
- Sandage, A. & Tammann, G. A. 1971, ApJ, 167, 293 (ST71)
- Sandage, A. 1972, QJRAS, 13, 202
- Sasselov, et al. 1997, A&A, 324, 471
- Simon, N. R. & Young, T. S. 1997, MNRAS, 288, 267
- Stobie, R. S. 1969, MNRAS, 144, 511
- Szabados, L., & Pont, F. 1998, A&AS, 133, 51
- Tanvir, N. 1997, in The Extragalactic Distance Scale, ed. M. Livio, M. Donahue & N. Panagia, (Cambridge Univ. Press: Cambridge), 91

van Genderen, A. M. 1974, *A&A*, 34, 279

van Genderen, A. M. 1978, *A&A*, 65, 147

Welch, D. L. et al. 1997, in *Variable Stars and the Astrophysical Returns of Microlensing Surveys*, ed. R. Ferlet, J.P. Maillard & B. Raban, (Editions Frontières: Gif-sur-Yvette Cedex), 205

Ya'ari, A., & Tuchman, Y. 1999, *ApJ*, 514, L35

This preprint was prepared with the AAS L^AT_EX macros v4.0.

Fig. 1.— Comparison between different ML relations. *Top Panel:* ML relations at solar chemical compositions provided by CWC93 (dashed line), by ABHA99 (long-dashed line) and by CCS92 (filled squares). These relations are based on evolutionary models which neglect convective core overshooting, while the open squares mimic the behavior of a ML relation which include the convective core overshooting. *Bottom panel:* Same as the top panel, but referred to ML relations derived by adopting different chemical compositions (see labeled values).

Fig. 2.— Instability strip for fundamental pulsators in the H-R diagram as a function of metal content. Solid and dashed lines refer to the blue and the red edge respectively. The edges of models based on the canonical ML relations are plotted as filled circles, while models based on the noncanonical ML relation with triangles. The error bars show the theoretical uncertainty (± 50 K) on the effective temperature of the edges.

Fig. 3.— Comparison in the H-R diagram between linear and nonlinear (solid lines) fundamental edges at fixed chemical composition (see labeled values). The edges estimated by CWC93 (dashed lines) and by ABHA99 (filled circles) are based on linear, nonadiabatic, convective models. See text for further details.

Fig. 4.— Distribution of first overtone pulsators (open circles) in the H-R diagram as a function of the metal content. The solid and the dashed lines show the edges of fundamental and first overtone pulsators respectively.

Fig. 5.— Predicted fundamental periods as a function of the effective temperature for both canonical (triangles) and noncanonical (squares) models at different chemical compositions and stellar masses (see labeled values). The solid lines refer to the fundamental periods obtained by adopting the analytical relations connecting the logarithmic period to $\log L$, $\log M$, and $\log T_e$.

Fig. 6.— Bolometric amplitudes for fundamental pulsators as a function of period. Solid and dashed lines refer to canonical and noncanonical models respectively. Models characterized by different stellar masses are plotted with different symbols. The three panels refer to models constructed by adopting different chemical compositions (see labeled values).

Fig. 7.— Comparison of theoretical amplitudes for $Z=0.008$ (solid lines) and $Z=0.02$ (dashed lines) with empirical amplitudes for Galactic Cepheids collected by Fernie et al. (1995) on the $\log P - A_V$ plane. The mass values are specified close to the amplitude sequences.

Fig. 8.— Amplitude ratio in the I (Cousins) and in the V (Johnson) bands for canonical, fundamental models versus period. From top to bottom the panels refer to models with

different chemical compositions (see labeled values).

Fig. 9.— Comparison between observed and theoretical radial velocity amplitudes as a function of period. Empirical radial velocity amplitudes were transformed into true pulsational amplitudes by adopting a projection factor of 1.36. Solid and dashed lines refer to sets of models constructed by adopting $Z=0.02$ and $Z=0.008$ respectively and to different stellar masses (see labeled values). *Top Panel:* Velocity amplitudes for Galactic Cepheids measured by Bersier et al. (1994) and by Bersier (1999, private communication). *Bottom Panel:* As the top panel but for velocity amplitudes collected by Cogan (1980).

Fig. 10.— First overtone pulsation amplitudes as function of the pulsation period. From top to bottom the panels show the bolometric and radial velocity amplitude, the fractional radius and temperature variations. From left to right the panels refer to different chemical compositions (see labeled values). Models of different stellar masses are plotted with different symbols.

Fig. 11.— Bolometric light curves (left panel) and velocity (right panel) curves as a function of the pulsation phase. The curves plotted in this figure refer to a sequence of models constructed at fixed mass, luminosity and chemical composition (see labeled values) and canonical ML relation. Dashed and solid lines show the luminosity and the velocity variation over two pulsation cycles of first overtone and fundamental pulsators respectively. In the left panel are also listed the nonlinear periods (d), while on the right panel the static effective temperatures (K). Positive values along the velocity curves denote expansion phases, while negative values denote contraction phases.

Fig. 12.— Similar to the previous figure, but for $M/M_{\odot}=7$ models.

Fig. 13.— Similar to the previous figure, but for $M/M_{\odot}=9$ models.

Fig. 14.— Similar to the previous figure, but for $M/M_{\odot}=11$ models.

Fig. 15.— As in Fig. 11, but for more metal-rich models ($Z=0.008$ against $Z=0.004$).

Fig. 16.— Similar to the previous figure, but for $M/M_{\odot}=7$ models.

Fig. 17.— Similar to the previous figure, but for $M/M_{\odot}=9$ models.

Fig. 18.— Similar to the previous figure, but for $M/M_{\odot}=1$ models.

Fig. 19.— As in Fig. 15, but for models constructed by adopting higher helium ($Y=0.28$ against $Y=0.25$) and metal ($Z=0.02$ against $Z=0.008$) contents.

Fig. 20.— Similar to the previous figure, but for $M/M_{\odot}=7$ models.

Fig. 21.— Similar to the previous figure, but for $M/M_{\odot}=9$ models.

Fig. 22.— Similar to the previous figure, but for $M/M_{\odot}=11$ models.

Fig. 23.— As in Fig. 11, but for models constructed by adopting a noncanonical ML relation.

Fig. 24.— Similar to the previous figure, but for $M/M_{\odot}=7$ models.

Fig. 25.— Similar to the previous figure, but for $M/M_{\odot}=9$ models.

Fig. 26.— Similar to the previous figure, but for $M/M_{\odot}=11$ models.

Fig. 27.— As in Fig. 15, but for models constructed by adopting a noncanonical ML relation.

Fig. 28.— Similar to the previous figure, but for $M/M_{\odot}=7$ models.

Fig. 29.— Similar to the previous figure, but for $M/M_{\odot}=9$ models.

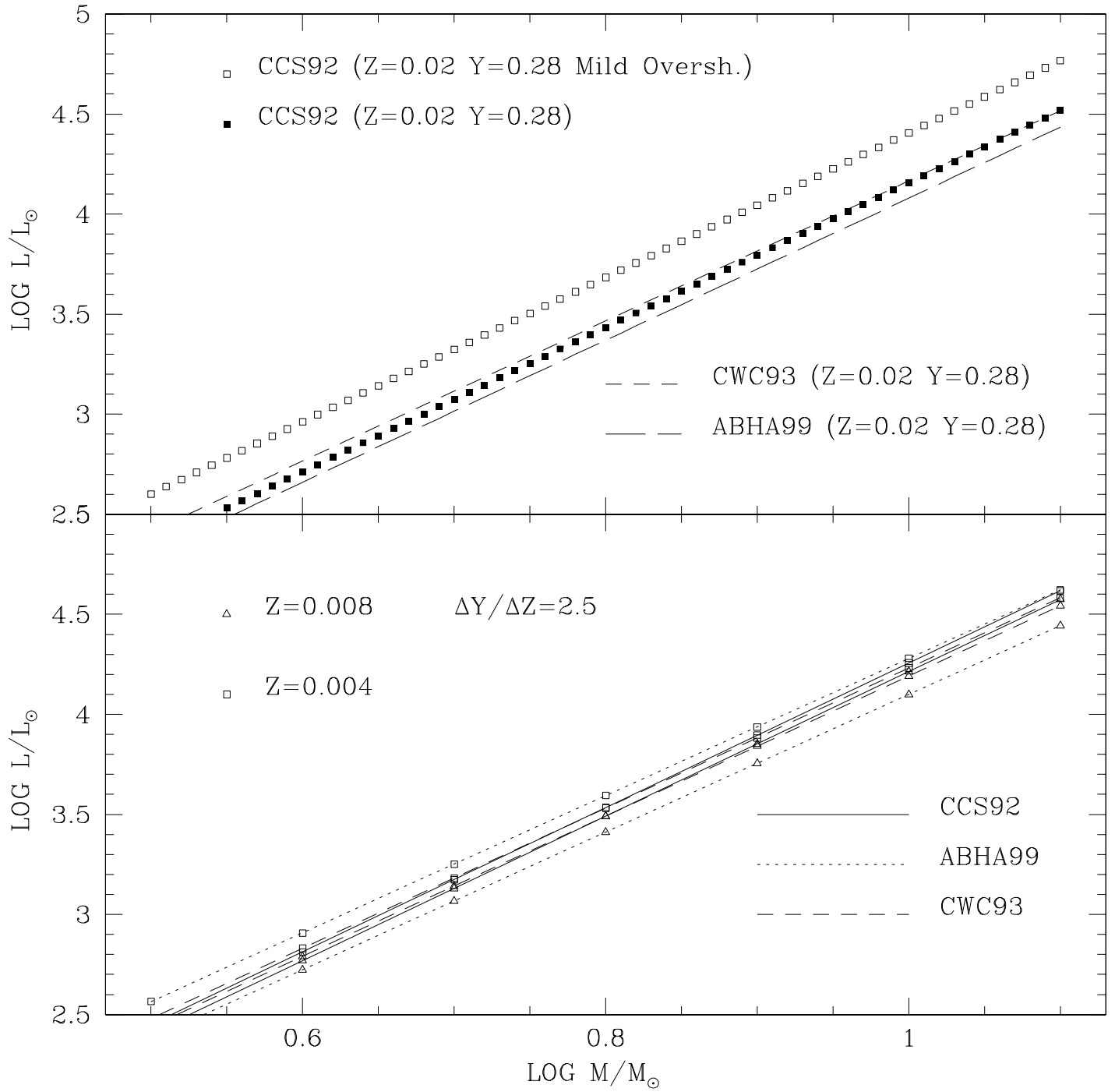
Fig. 30.— Similar to the previous figure, but for $M/M_{\odot}=11$ models.

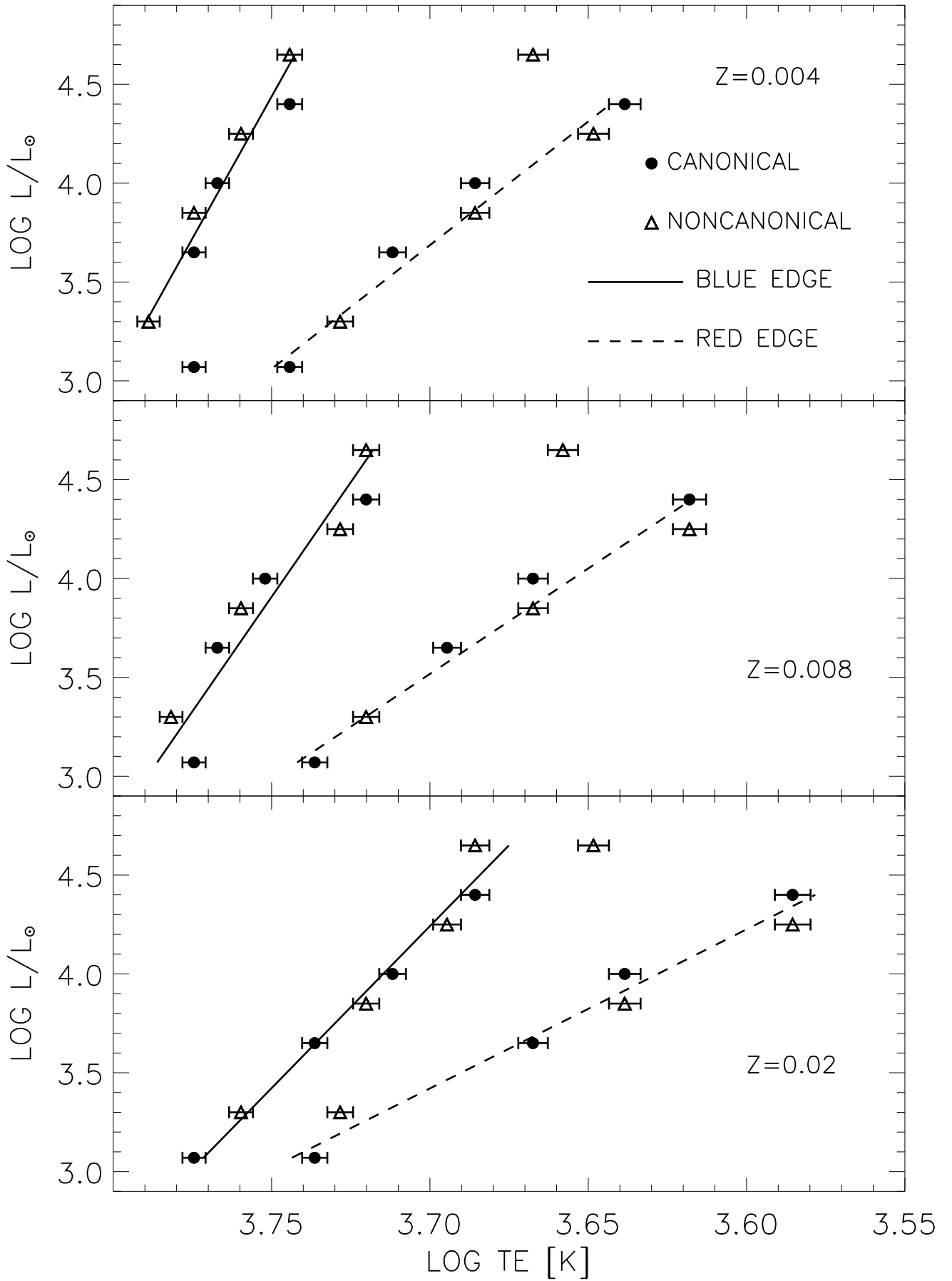
Fig. 31.— As in Fig. 19, but for models constructed by adopting a noncanonical ML relation.

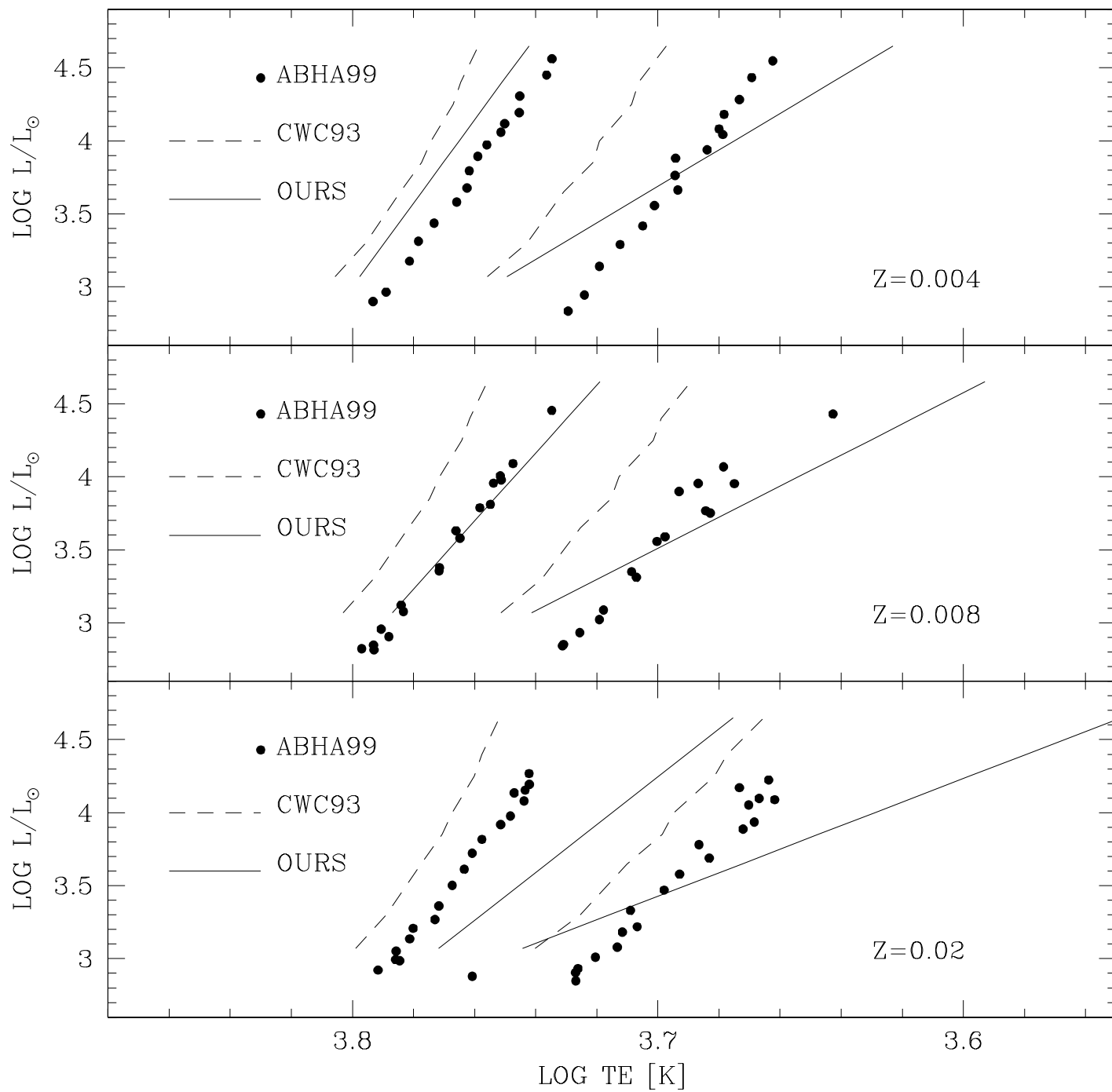
Fig. 32.— Similar to the previous figure, but for $M/M_{\odot}=7$ models.

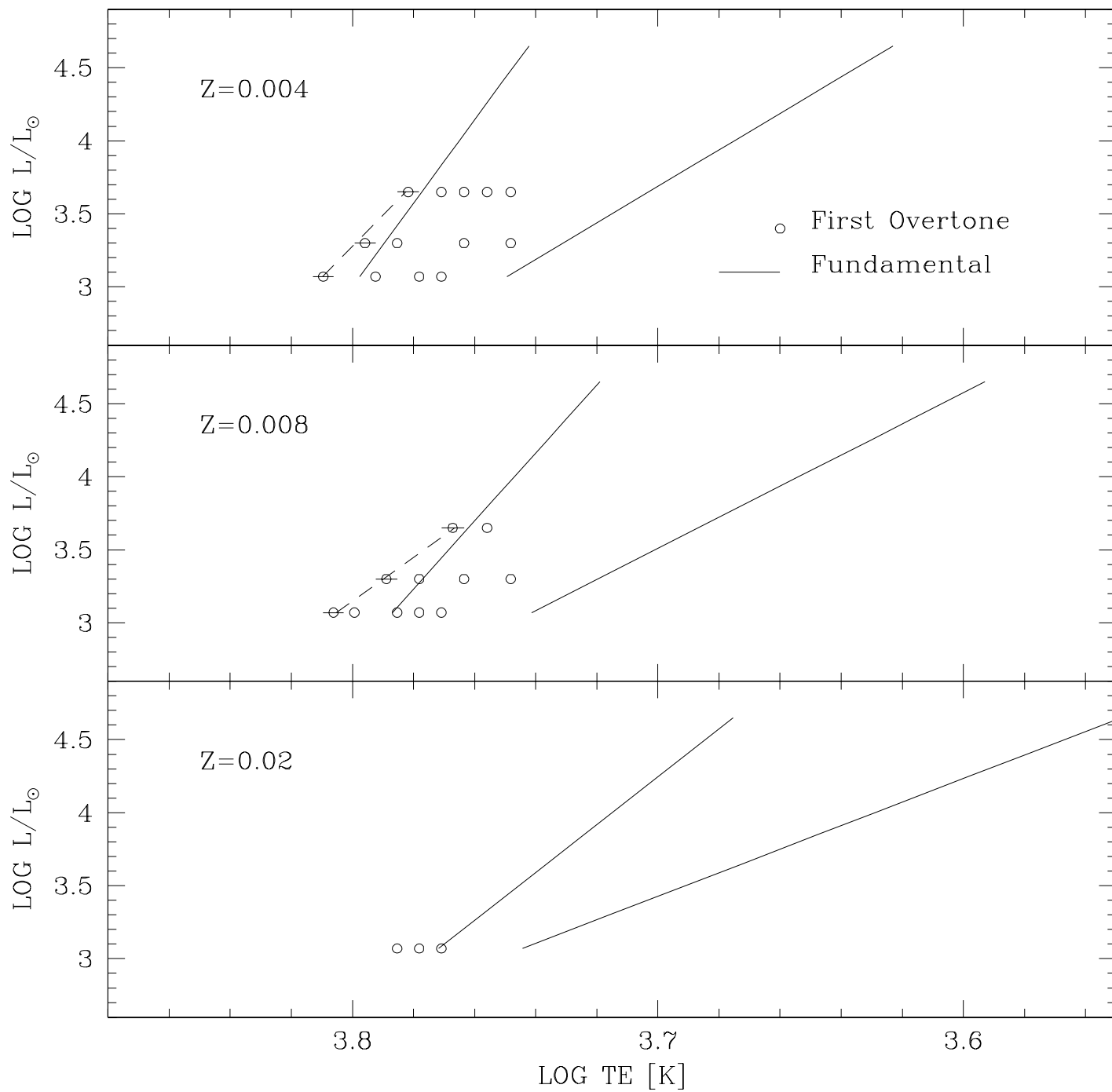
Fig. 33.— Similar to the previous figure, but for $M/M_{\odot}=9$ models.

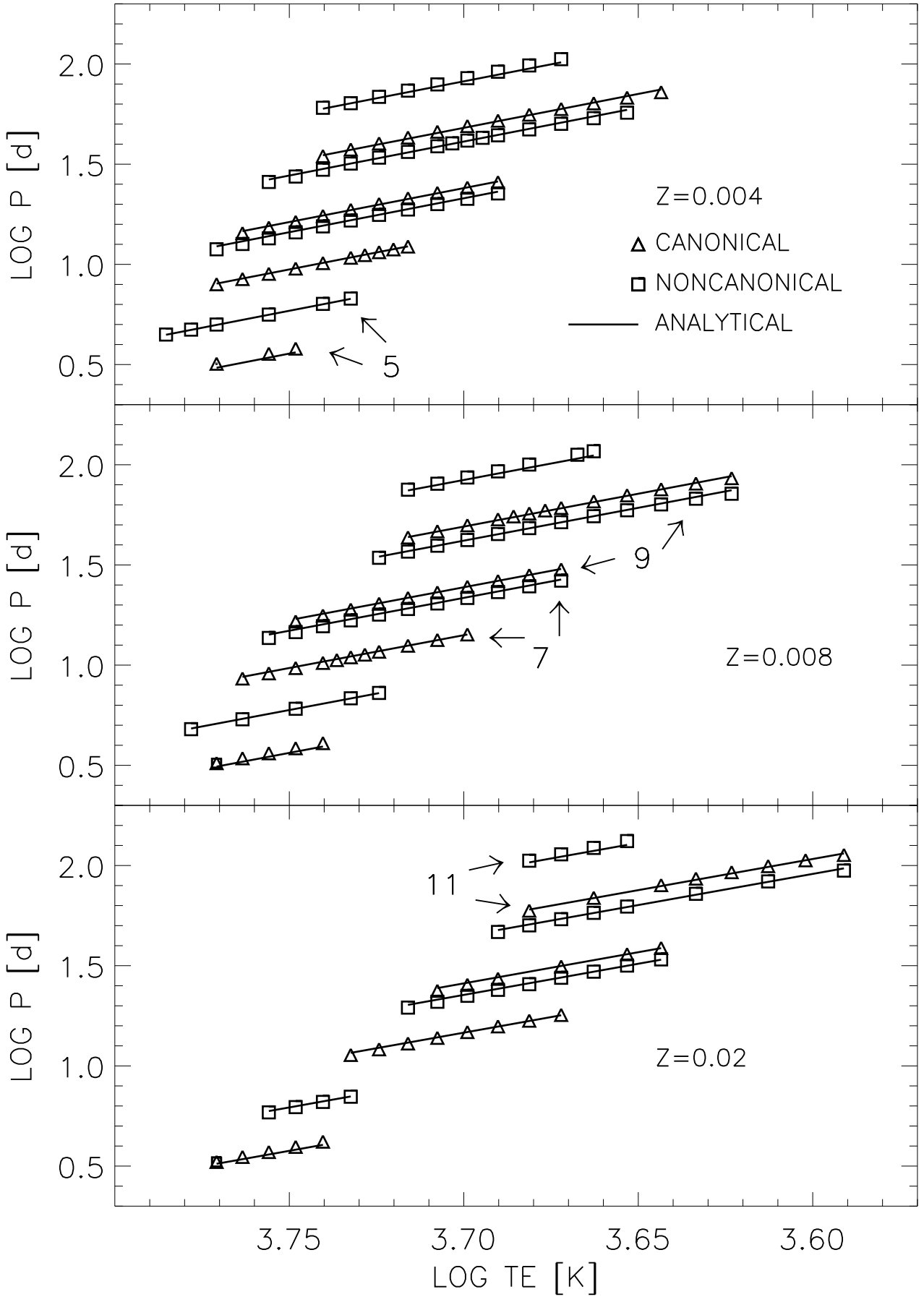
Fig. 34.— Similar to the previous figure, but for $M/M_{\odot}=11$ models.

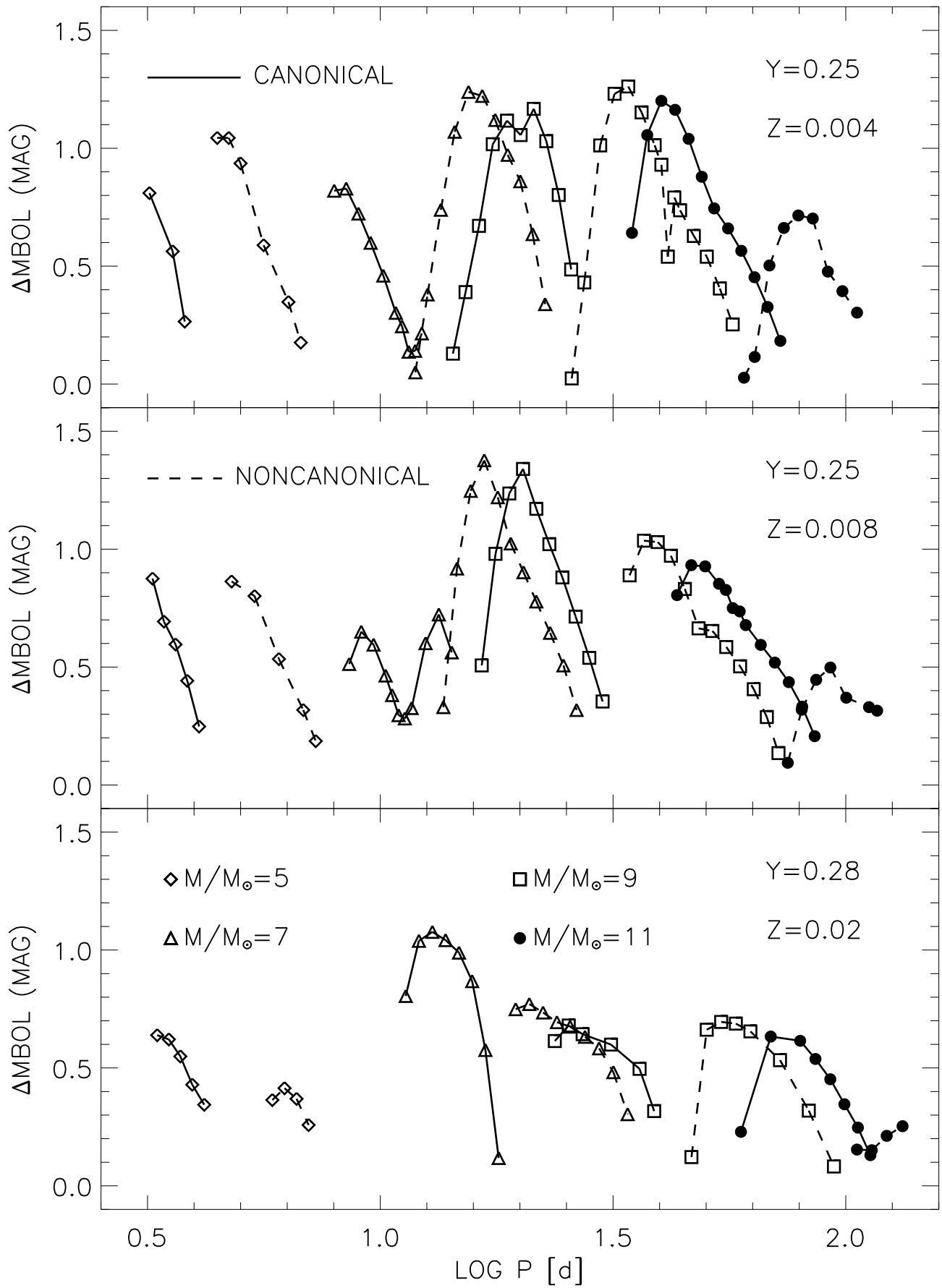


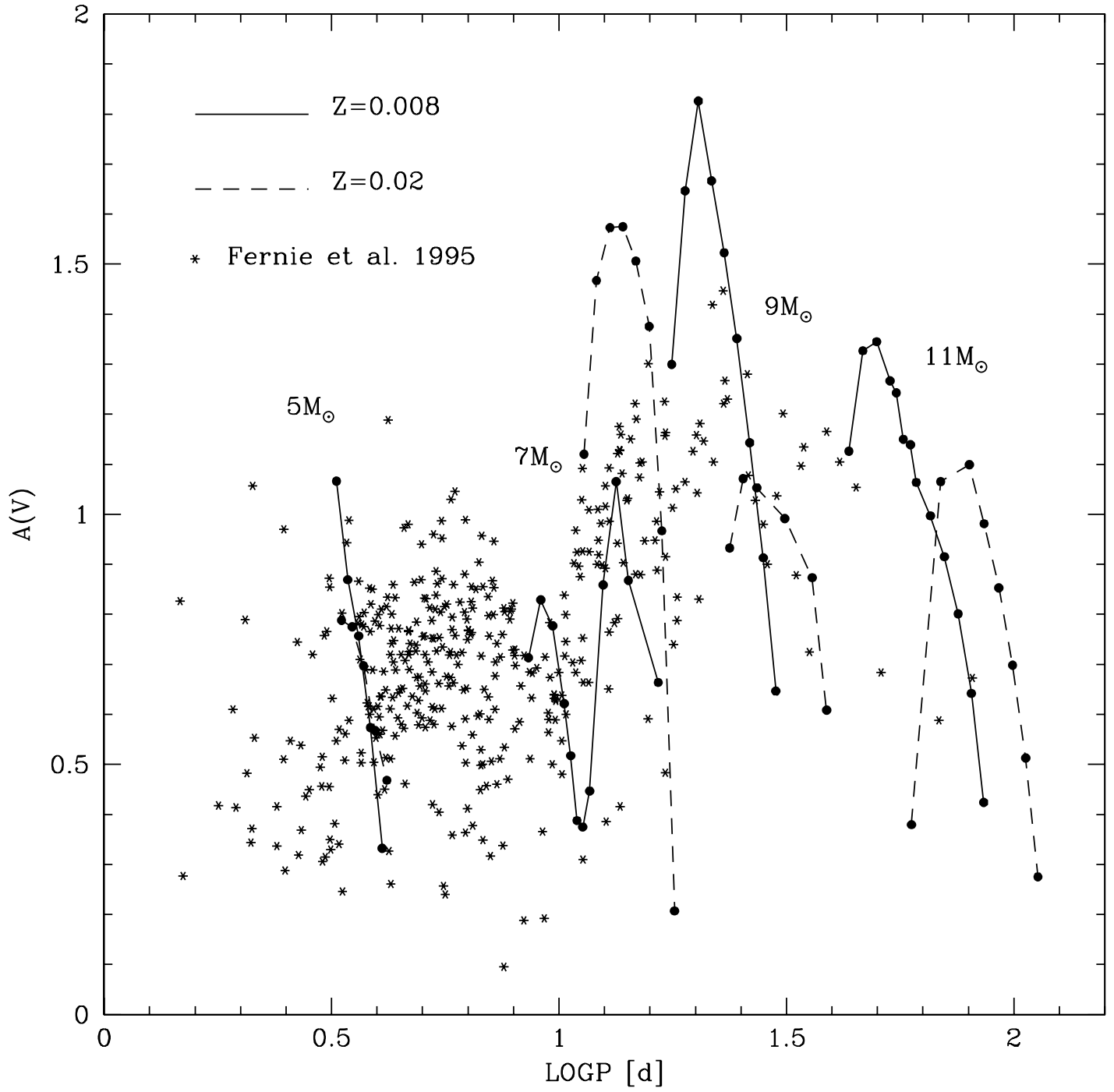


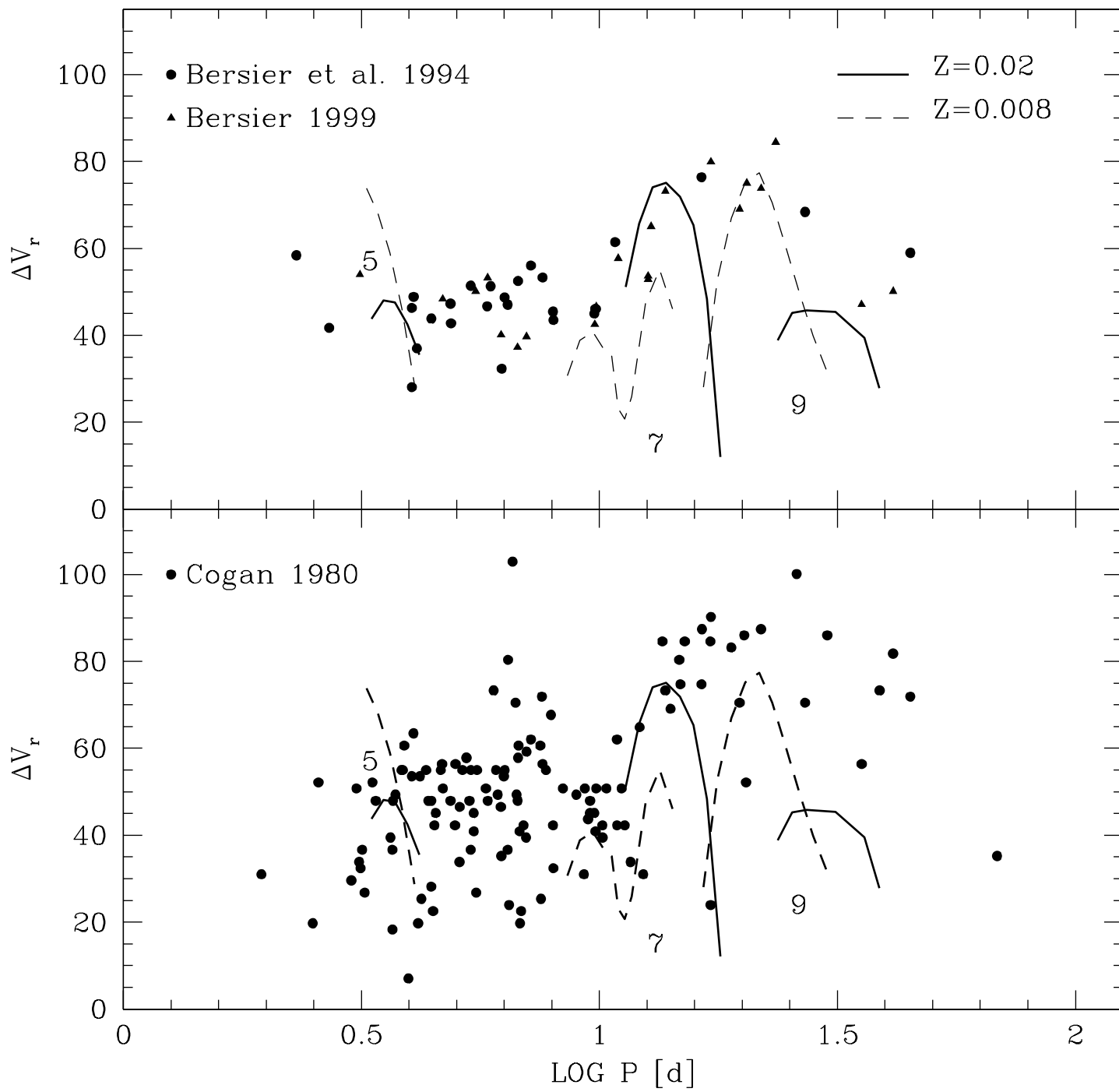


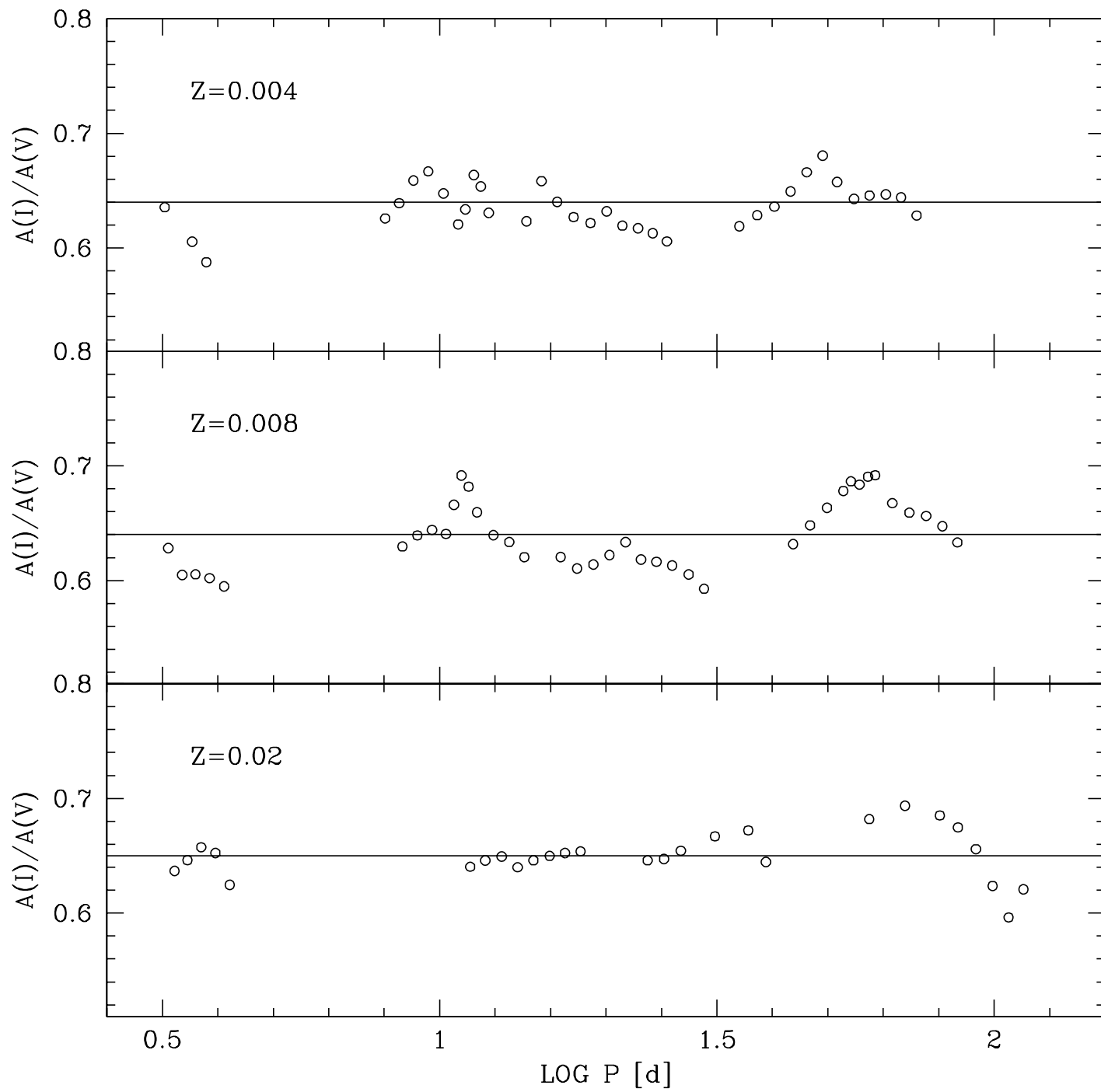












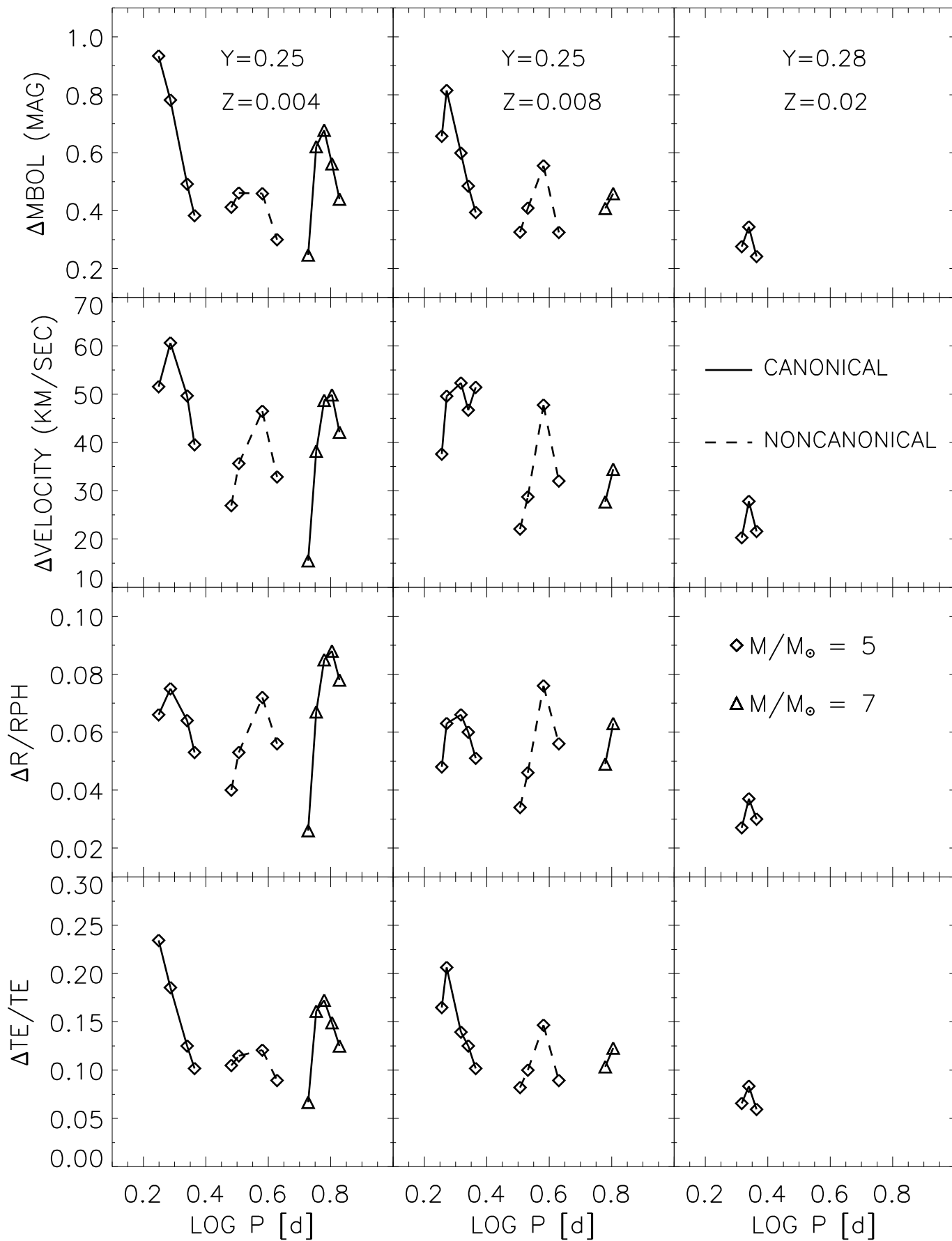


TABLE 1
FIRST OVERTONE PULSATORS (CANONICAL ML RELATION).

M^a	$\log L^b$	T_e^c	P^d	$\log \bar{R}^e$	$\Delta R/R_{ph}^f$	Δu^g	ΔM_{bol}^h	$\Delta \log g_s^i$	$\Delta \log g_e^j$	ΔT^k	ΔT_e^l	KE^m
(1)	(2)	(3)	(4)	(5)	(6)	(7)	(8)	(9)	(10)	(11)	(12)	(13)
Y=0.25 Z=0.004												
5.0	3.07	6400	1.7732	1.450	0.066	51.55	0.934	0.06	0.73	1200	1500	2.418(40)
5.0	3.07	6200	1.9338	1.477	0.075	60.62	0.782	0.06	0.79	950	1150	4.458(40)
5.0	3.07	6000	2.1879	1.505	0.064	49.66	0.492	0.06	0.64	600	750	1.960(40)
5.0	3.07	5900	2.3107	1.518	0.053	39.53	0.383	0.05	0.50	500	600	8.535(39)
7.0	3.65	6000	5.3420	1.794	0.026	15.50	0.247	0.02	0.21	300	400	5.640(39)
7.0	3.65	5900	5.6686	1.810	0.067	38.20	0.621	0.06	0.55	750	950	3.606(40)
7.0	3.65	5800	6.0112	1.826	0.085	48.72	0.678	0.07	0.71	800	1000	8.991(40)
7.0	3.65	5700	6.3668	1.842	0.088	49.86	0.562	0.08	0.72	700	850	1.175(41)
7.0	3.65	5600	6.7294	1.855	0.078	42.12	0.440	0.07	0.62	550	700	8.649(40)
Y=0.25 Z=0.008												
5.0	3.07	6370	1.8014	1.453	0.048	37.59	0.657	0.04	0.49	850	1050	1.268(40)
5.0	3.07	6300	1.8682	1.463	0.063	49.58	0.815	0.05	0.65	1050	1300	2.346(40)
5.0	3.07	6100	2.0758	1.491	0.066	52.32	0.599	0.06	0.66	700	850	2.280(40)
5.0	3.07	6000	2.1905	1.505	0.060	46.70	0.485	0.05	0.59	600	750	1.445(40)
5.0	3.07	5900	2.3139	1.519	0.051	51.42	0.394	0.04	0.48	500	600	7.305(39)
7.0	3.65	5800	6.0167	1.825	0.049	27.70	0.408	0.04	0.38	500	600	2.692(40)
7.0	3.65	5700	6.3789	1.840	0.063	34.46	0.459	0.05	0.49	550	700	4.815(40)
Y=0.28 Z=0.02												
5.0	3.07	6100	2.0731	1.490	0.027	20.28	0.276	0.02	0.24	350	400	2.011(39)
5.0	3.07	6000	2.1847	1.504	0.037	27.80	0.344	0.03	0.33	400	500	3.335(39)
5.0	3.07	5900	2.3122	1.519	0.030	21.58	0.242	0.03	0.26	300	350	1.569(39)

^a Stellar mass (solar units). ^b Logarithmic luminosity (solar units). ^c Effective temperature (K). ^d Period (day). ^e Logarithmic mean radius (solar units). ^f Fractional radius variation. ^g Radial velocity amplitude (Kms^{-1}). ^h Bolometric amplitude (mag). ⁱ Amplitude of logarithmic static gravity. ^j Amplitude of logarithmic effective gravity. ^k Surface temperature variation (K). ^l Effective temperature variation (K). ^m Total kinetic energy (erg).

TABLE 2
 FUNDAMENTAL PULSATORS (CANONICAL ML RELATION).

M^a	$\log L^b$	T_e^c	P^d	$\log \bar{R}^e$	$\Delta R/R_{ph}^f$	Δu^g	ΔM_{bol}^h	$\Delta \log g_s^i$	$\Delta \log g_e^j$	ΔT^k	ΔT_e^l	KE^m
(1)	(2)	(3)	(4)	(5)	(6)	(7)	(8)	(9)	(10)	(11)	(12)	(13)
Y=0.25 Z=0.004												
5.0	3.07	5900	3.1920	1.523	0.152	82.34	0.810	0.13	0.91	1050	1300	3.734(41)
5.0	3.07	5700	3.5812	1.549	0.119	60.12	0.563	0.10	0.67	800	950	1.806(41)
5.0	3.07	5600	3.8008	1.561	0.067	32.78	0.265	0.06	0.33	400	500	1.935(40)
7.0	3.65	5900	7.9616	1.811	0.099	42.44	0.820	0.09	0.52	1000	1200	2.549(41)
7.0	3.65	5800	8.4499	1.826	0.111	49.91	0.829	0.10	0.56	950	1200	3.099(41)
7.0	3.65	5700	8.9766	1.841	0.110	50.23	0.723	0.10	0.59	800	950	3.732(41)
7.0	3.65	5600	9.5358	1.855	0.100	45.59	0.599	0.09	0.56	650	800	2.941(41)
7.0	3.65	5500	10.1497	1.869	0.093	41.48	0.460	0.08	0.49	550	650	3.815(41)
7.0	3.65	5400	10.7996	1.883	0.072	29.72	0.302	0.06	0.37	400	500	2.326(41)
7.0	3.65	5350	11.1330	1.890	0.062	24.38	0.245	0.05	0.32	300	400	1.843(41)
7.0	3.65	5300	11.5081	1.896	0.036	12.55	0.137	0.03	0.18	200	250	4.106(40)
7.0	3.65	5250	11.8828	1.904	0.035	13.22	0.141	0.03	0.17	200	200	1.189(40)
7.0	3.65	5200	12.2781	1.912	0.051	20.43	0.215	0.05	0.23	300	250	1.120(40)
9.0	4.00	5800	14.3252	1.999	0.019	6.92	0.129	0.02	0.08	150	200	8.904(39)
9.0	4.00	5700	15.2461	2.014	0.066	22.20	0.390	0.06	0.34	400	500	8.362(40)
9.0	4.00	5600	16.2950	2.031	0.104	39.72	0.671	0.09	0.50	800	950	1.881(41)
9.0	4.00	5500	17.4438	2.049	0.151	58.44	1.017	0.13	0.78	1200	1450	6.149(41)
9.0	4.00	5400	18.7160	2.069	0.191	71.31	1.117	0.16	1.06	1350	1650	1.258(42)
9.0	4.00	5300	20.0209	2.087	0.223	80.35	1.056	0.19	1.16	1300	1600	2.168(42)
9.0	4.00	5200	21.3641	2.103	0.233	80.88	1.167	0.20	1.15	1400	1750	2.996(42)
9.0	4.00	5100	22.7370	2.115	0.216	70.62	1.030	0.19	0.95	1250	1550	1.405(42)
9.0	4.00	5000	24.1723	2.127	0.185	56.39	0.802	0.16	0.77	1000	1250	7.006(41)
9.0	4.00	4900	25.7072	2.137	0.134	38.07	0.486	0.12	0.51	650	800	2.893(41)
11.0	4.40	5500	34.7262	2.249	0.131	32.20	0.641	0.23	0.53	800	1000	1.485(42)
11.0	4.40	5400	37.4530	2.270	0.216	51.31	1.056	0.30	0.93	1250	1550	3.658(42)
11.0	4.40	5300	40.1659	2.288	0.246	58.89	1.201	0.34	1.03	1350	1650	4.436(42)
11.0	4.40	5200	42.9870	2.304	0.254	60.88	1.163	0.37	1.00	1200	1500	4.562(42)
11.0	4.40	5100	45.9495	2.319	0.250	59.61	1.040	0.40	0.95	1050	1300	4.541(42)
11.0	4.40	5000	49.0565	2.333	0.235	55.46	0.879	0.43	0.88	900	1100	4.297(42)
11.0	4.40	4900	52.1530	2.345	0.216	49.37	0.745	0.45	0.79	850	1000	3.453(42)
11.0	4.40	4800	55.8722	2.359	0.194	43.16	0.660	0.47	0.69	750	900	2.673(42)
11.0	4.40	4700	59.6443	2.379	0.171	37.04	0.565	0.49	0.59	600	750	1.919(42)
11.0	4.40	4600	63.6795	2.385	0.145	30.40	0.453	0.51	0.48	500	650	1.226(42)
11.0	4.40	4500	67.9329	2.397	0.115	23.30	0.327	0.52	0.36	400	450	6.507(41)
11.0	4.40	4400	72.3487	2.409	0.075	14.47	0.183	0.53	0.22	250	300	2.539(41)
Y=0.25 Z=0.008												
5.0	3.07	5900	3.2417	1.523	0.136	73.80	0.875	0.12	0.80	1050	1300	2.982(42)
5.0	3.07	5800	3.4292	1.536	0.130	68.01	0.693	0.11	0.75	950	1150	2.991(41)
5.0	3.07	5700	3.6315	1.550	0.117	58.94	0.596	0.10	0.64	800	1000	1.440(41)
5.0	3.07	5600	3.8487	1.563	0.095	46.10	0.442	0.08	0.48	600	750	4.500(40)
5.0	3.07	5500	4.0813	1.576	0.061	28.81	0.248	0.05	0.29	350	450	1.126(40)
7.0	3.65	5800	8.5734	1.824	0.066	30.71	0.513	0.06	0.34	650	850	8.266(40)
7.0	3.65	5700	9.1025	1.840	0.089	38.84	0.650	0.08	0.45	750	900	2.591(40)

TABLE 2—*Continued*

M^a	$\log L^b$	T_e^c	P^d	$\log \bar{R}_t^e$	$\Delta R/R_{ph}^f$	Δu^g	ΔM_{bol}^h	$\Delta \log g_s^i$	$\Delta \log g_e^j$	ΔT^k	ΔT_e^l	KE^m
(1)	(2)	(3)	(4)	(5)	(6)	(7)	(8)	(9)	(10)	(11)	(12)	(13)
7.0	3.65	5600	9.6741	1.856	0.094	40.83	0.595	0.08	0.48	700	850	2.433(41)
7.0	3.65	5500	10.2660	1.869	0.087	36.43	0.464	0.08	0.45	550	650	2.691(41)
7.0	3.65	5450	10.6009	1.877	0.080	35.15	0.381	0.07	0.42	500	550	2.395(41)
7.0	3.65	5400	10.9473	1.884	0.062	23.18	0.296	0.05	0.33	350	400	1.227(41)
7.0	3.65	5350	11.2904	1.892	0.058	20.75	0.282	0.05	0.31	300	350	8.270(40)
7.0	3.65	5300	11.6768	1.899	0.064	25.89	0.326	0.06	0.34	350	450	3.036(40)
7.0	3.65	5200	12.5072	1.918	0.113	47.61	0.601	0.10	0.57	700	850	8.099(40)
7.0	3.65	5100	13.3591	1.935	0.140	55.15	0.723	0.12	0.69	850	1050	1.432(41)
7.0	3.65	5000	14.2372	1.949	0.131	46.10	0.562	0.12	0.58	700	850	1.553(41)
9.0	4.00	5600	16.5176	2.030	0.080	28.06	0.507	0.07	0.33	600	750	2.063(41)
9.0	4.00	5500	17.6816	2.050	0.147	52.86	0.980	0.13	0.68	1200	1500	7.027(41)
9.0	4.00	5400	18.9332	2.069	0.191	66.91	1.236	0.16	0.96	1500	1900	1.360(42)
9.0	4.00	5300	20.2593	2.088	0.221	75.24	1.340	0.19	1.11	1600	1950	2.018(42)
9.0	4.00	5200	21.6398	2.104	0.231	77.42	1.171	0.20	1.02	1350	1650	1.637(42)
9.0	4.00	5100	23.0796	2.118	0.222	70.52	1.021	0.19	0.95	1250	1550	1.125(42)
9.0	4.00	5000	24.6201	2.132	0.204	60.43	0.880	0.18	0.86	1100	1350	6.842(41)
9.0	4.00	4900	26.2864	2.145	0.181	49.98	0.714	0.16	0.74	900	1100	4.545(41)
9.0	4.00	4800	28.1229	2.160	0.158	39.90	0.539	0.14	0.63	700	900	3.145(41)
9.0	4.00	4700	30.0358	2.173	0.130	31.64	0.354	0.12	0.47	500	650	3.282(41)
11.0	4.40	5200	43.4044	2.299	0.177	40.32	0.805	0.34	0.66	900	1150	1.888(42)
11.0	4.40	5100	46.5814	2.318	0.212	47.21	0.932	0.39	0.79	1000	1250	2.617(42)
11.0	4.40	5000	49.8826	2.327	0.221	49.22	0.927	0.43	0.78	950	1150	3.072(42)
11.0	4.40	4900	53.4119	2.350	0.218	48.63	0.853	0.46	0.76	850	1050	2.991(42)
11.0	4.40	4850	55.2678	2.358	0.217	48.51	0.827	0.47	0.76	800	1000	3.064(42)
11.0	4.40	4800	57.1738	2.352	0.206	45.34	0.750	0.48	0.71	750	900	2.645(42)
11.0	4.40	4750	59.1773	2.373	0.204	44.98	0.736	0.49	0.71	750	900	2.631(42)
11.0	4.40	4700	60.9618	2.379	0.196	42.49	0.678	0.51	0.67	700	850	2.372(42)
11.0	4.40	4600	65.6808	2.394	0.180	38.51	0.594	0.54	0.60	600	750	2.004(42)
11.0	4.40	4500	70.4054	2.409	0.161	34.11	0.519	0.56	0.53	550	650	1.622(42)
11.0	4.40	4400	75.4589	2.423	0.139	28.81	0.436	0.58	0.44	450	550	1.178(42)
11.0	4.40	4300	80.6113	2.436	0.112	22.47	0.332	0.60	0.34	350	450	7.290(41)
11.0	4.40	4200	85.7446	2.447	0.079	15.10	0.207	0.61	0.23	250	300	3.011(41)
Y=0.28 Z=0.02												
5.0	3.07	5900	3.3169	1.520	0.085	43.74	0.639	0.07	0.43	800	950	4.841(40)
5.0	3.07	5800	3.5140	1.535	0.095	48.08	0.621	0.08	0.49	750	900	5.496(40)
5.0	3.07	5700	3.7190	1.549	0.096	47.62	0.549	0.08	0.49	650	800	4.998(40)
5.0	3.07	5600	3.9453	1.564	0.089	42.48	0.429	0.08	0.44	550	700	3.377(40)
5.0	3.07	5500	4.1863	1.579	0.077	35.57	0.344	0.07	0.37	450	550	1.902(40)
7.0	3.65	5400	11.3422	1.889	0.131	51.12	0.805	0.11	0.55	950	1200	1.342(41)
7.0	3.65	5300	12.1039	1.908	0.168	65.67	1.039	0.14	0.76	1200	1500	2.445(41)
7.0	3.65	5200	12.9389	1.927	0.194	74.01	1.077	0.17	0.91	1250	1550	3.582(41)
7.0	3.65	5100	13.8115	1.945	0.206	75.13	1.042	0.18	0.98	1250	1550	4.371(41)
7.0	3.65	5000	14.7615	1.961	0.208	71.84	0.989	0.18	0.94	1200	1450	6.131(41)
7.0	3.65	4900	15.7542	1.976	0.196	65.34	0.868	0.17	0.82	1000	1250	5.824(41)
7.0	3.65	4800	16.8212	1.988	0.155	48.38	0.576	0.14	0.58	700	850	2.660(41)

TABLE 2—*Continued*

M^a	$\log L^b$	T_e^c	P^d	$\log \bar{R}^e$	$\Delta R/R_{ph}^f$	Δu^g	ΔM_{bol}^h	$\Delta \log g_s^i$	$\Delta \log g_e^j$	ΔT^k	ΔT_e^l	KE^m
(1)	(2)	(3)	(4)	(5)	(6)	(7)	(8)	(9)	(10)	(11)	(12)	(13)
7.0	3.65	4700	17.9605	2.000	0.042	12.08	0.118	0.04	0.14	150	200	1.282(40)
9.0	4.00	5100	23.7088	2.114	0.141	38.80	0.614	0.12	0.51	750	900	3.653(41)
9.0	4.00	5000	25.4006	2.132	0.171	45.22	0.680	0.15	0.65	850	1050	4.112(41)
9.0	4.00	4900	27.2110	2.150	0.182	45.79	0.643	0.16	0.69	800	950	4.406(41)
9.0	4.00	4700	31.3104	2.185	0.192	45.35	0.599	0.16	0.69	700	850	6.551(41)
9.0	4.00	4500	36.0629	2.217	0.172	39.48	0.496	0.18	0.58	550	700	6.327(41)
9.0	4.00	4400	38.7582	2.230	0.124	27.87	0.317	0.19	0.40	400	450	3.497(41)
11.0	4.40	4800	59.5490	2.363	0.070	13.73	0.229	0.44	0.19	250	300	1.544(41)
11.0	4.40	4600	69.0000	2.402	0.177	34.61	0.633	0.55	0.54	600	750	1.344(42)
11.0	4.40	4400	79.8194	2.435	0.177	35.14	0.615	0.62	0.54	550	650	1.689(42)
11.0	4.40	4300	86.0767	2.451	0.162	31.49	0.538	0.64	0.48	450	600	1.538(42)
11.0	4.40	4200	92.6401	2.466	0.142	27.10	0.452	0.67	0.43	400	500	1.310(42)
11.0	4.40	4100	99.3362	2.480	0.117	21.64	0.346	0.69	0.35	300	400	1.182(42)
11.0	4.40	4000	106.1928	2.493	0.086	15.49	0.247	0.70	0.25	250	300	1.115(42)
11.0	4.40	3900	112.9544	2.503	0.048	8.43	0.130	0.71	0.13	150	150	5.137(41)

^a Stellar mass (solar units). ^b Logarithmic luminosity (solar units). ^c Effective temperature (K). ^d Period (day).
^e Logarithmic mean radius (solar units). ^f Fractional radius variation. ^g Radial velocity amplitude (Kms⁻¹).
^h Bolometric amplitude (mag). ⁱ Amplitude of logarithmic static gravity. ^j Amplitude of logarithmic effective gravity. ^k Surface temperature variation (K). ^l Effective temperature variation (K). ^m Total kinetic energy (erg).

TABLE 3
FIRST OVERTONE PULSATORS (NONCANONICAL ML RELATION).

M^a	$\log L^b$	T_e^c	P^d	$\log \bar{R}^e$	$\Delta R/R_{ph}^f$	Δu^g	ΔM_{bol}^h	$\Delta \log g_s^i$	$\Delta \log g_e^j$	ΔT^k	ΔT_e^l	KE^m
(1)	(2)	(3)	(4)	(5)	(6)	(7)	(8)	(9)	(10)	(11)	(12)	(13)
Y=0.25 Z=0.004												
5.0	3.30	6200	3.0308	1.592	0.040	26.92	0.412	0.03	0.35	500	650	4.633(39)
5.0	3.30	6100	3.2039	1.606	0.053	35.63	0.461	0.05	0.50	550	700	7.077(39)
5.0	3.30	5800	3.8107	1.650	0.072	46.48	0.459	0.06	0.60	550	700	1.333(40)
5.0	3.30	5600	4.2466	1.677	0.056	32.86	0.300	0.05	0.44	400	500	1.073(40)
Y=0.25 Z=0.008												
5.0	3.30	6100	3.2094	1.605	0.034	22.07	0.326	0.03	0.30	400	500	1.996(39)
5.0	3.30	6000	3.3994	1.620	0.046	28.72	0.409	0.04	0.41	500	600	3.695(39)
5.0	3.30	5800	3.8160	1.651	0.076	47.74	0.555	0.07	0.61	650	850	1.612(40)
5.0	3.30	5600	4.2726	1.678	0.056	32.01	0.325	0.05	0.43	400	500	9.831(39)

^a Stellar mass (solar units). ^b Logarithmic luminosity (solar units). ^c Effective temperature (K). ^d Period (day). ^e Logarithmic mean radius (solar units). ^f Fractional radius variation. ^g Radial velocity amplitude (Kms⁻¹). ^h Bolometric amplitude (mag). ⁱ Amplitude of logarithmic static gravity. ^j Amplitude of logarithmic effective gravity. ^k Surface temperature variation (K). ^l Effective temperature variation (K). ^m Total kinetic energy (erg).

TABLE 4
 FUNDAMENTAL PULSATORS (NONCANONICAL ML RELATION).

M^a	$\log L^b$	T_e^c	P^d	$\log \bar{R}^e$	$\Delta R/R_{ph}^f$	Δu^g	ΔM_{bol}^h	$\Delta \log g_s^i$	$\Delta \log g_e^j$	ΔT^k	ΔT_e^l	KE^m
(1)	(2)	(3)	(4)	(5)	(6)	(7)	(8)	(9)	(10)	(11)	(12)	(13)
Y=0.25 Z=0.004												
5.0	3.30	6100	4.4638	1.607	0.112	50.97	1.044	0.10	0.67	1300	1600	2.022(41)
5.0	3.30	6000	4.7249	1.623	0.127	60.38	1.044	0.11	0.72	1250	1550	2.362(41)
5.0	3.30	5900	5.0102	1.637	0.130	62.13	0.936	0.11	0.72	1050	1300	1.975(41)
5.0	3.30	5700	5.6156	1.665	0.115	54.03	0.589	0.10	0.63	700	850	1.064(41)
5.0	3.30	5500	6.3499	1.692	0.077	33.32	0.348	0.07	0.39	450	550	8.231(40)
5.0	3.30	5400	6.7478	1.705	0.045	19.46	0.176	0.04	0.20	250	300	1.324(39)
7.0	3.85	5900	11.8936	1.910	0.008	2.78	0.050	0.01	0.04	50	100	3.051(39)
7.0	3.85	5800	12.6386	1.925	0.060	19.82	0.380	0.05	0.30	400	500	2.583(40)
7.0	3.85	5700	13.4916	1.941	0.109	39.33	0.739	0.09	0.54	850	1050	1.083(41)
7.0	3.85	5600	14.4477	1.959	0.155	57.12	1.070	0.13	0.80	1300	1600	3.565(41)
7.0	3.85	5500	15.4727	1.978	0.196	70.16	1.239	0.17	1.08	1550	1900	7.756(41)
7.0	3.85	5400	16.5601	1.996	0.228	79.75	1.222	0.20	1.22	1450	1750	1.314(42)
7.0	3.85	5300	17.6617	2.012	0.235	80.13	1.120	0.20	1.12	1400	1700	1.447(42)
7.0	3.85	5200	18.7844	2.025	0.228	68.70	0.972	0.21	1.06	1300	1600	1.737(42)
7.0	3.85	5100	19.9887	2.036	0.198	58.45	0.860	0.17	0.86	1100	1350	4.405(41)
7.0	3.85	5000	21.2514	2.048	0.162	44.70	0.636	0.15	0.68	850	1050	2.302(41)
7.0	3.85	4900	22.6022	2.059	0.110	27.75	0.339	0.10	0.42	500	600	9.621(40)
9.0	4.25	5700	25.7807	2.140	0.004	1.12	0.024	0.04	0.21	50	50	4.523(38)
9.0	4.25	5600	27.4353	2.156	0.085	21.81	0.431	0.07	0.34	550	650	3.921(41)
9.0	4.25	5500	29.6773	2.178	0.204	48.30	1.012	0.18	0.91	1250	1550	1.956(42)
9.0	4.25	5400	31.8640	2.197	0.249	59.07	1.231	0.22	1.09	1450	1800	2.809(42)
9.0	4.25	5300	34.0954	2.214	0.264	63.69	1.262	0.23	1.08	1400	1700	3.034(42)
9.0	4.25	5200	36.4212	2.230	0.263	63.74	1.152	0.23	1.02	1200	1500	2.930(42)
9.0	4.25	5100	38.8574	2.244	0.253	60.83	1.013	0.25	0.98	1000	1200	3.005(42)
9.0	4.25	5050	40.1676	2.250	0.245	58.31	0.930	0.26	0.94	1000	1200	2.833(42)
9.0	4.25	5000	41.4628	2.256	0.164	35.00	0.540	0.27	0.89	950	1150	2.611(42)
9.0	4.25	4950	42.8265	2.263	0.224	51.29	0.791	0.28	0.84	900	1100	2.286(42)
9.0	4.25	4900	44.0638	2.268	0.210	47.01	0.737	0.29	0.76	850	1000	1.944(42)
9.0	4.25	4800	47.1567	2.282	0.184	40.04	0.628	0.31	0.65	700	900	1.377(42)
9.0	4.25	4700	50.2887	2.295	0.164	35.00	0.540	0.33	0.56	600	750	1.046(42)
9.0	4.25	4600	53.6414	2.307	0.134	27.61	0.405	0.35	0.44	500	600	6.043(41)
9.0	4.25	4500	57.1679	2.319	0.096	18.97	0.253	0.36	0.29	300	400	2.660(41)
11.0	4.65	5500	60.4344	2.371	0.005	1.02	0.027	0.43	0.02	50	50	9.056(39)
11.0	4.65	5400	63.7238	2.386	0.025	5.29	0.115	0.47	0.08	100	150	7.320(40)
11.0	4.65	5300	68.5561	2.405	0.119	23.75	0.503	0.54	0.38	600	700	1.208(42)
11.0	4.65	5200	73.6106	2.422	0.150	29.89	0.662	0.58	0.49	800	900	2.014(42)
11.0	4.65	5100	79.0768	2.438	0.162	32.19	0.715	0.61	0.56	850	950	2.650(42)
11.0	4.65	5000	84.9395	2.454	0.161	32.45	0.702	0.64	0.55	700	850	2.824(42)
11.0	4.65	4900	91.5153	2.465	0.128	24.62	0.477	0.66	0.43	500	650	2.111(42)
11.0	4.65	4800	98.3615	2.480	0.112	20.69	0.394	0.69	0.39	400	500	3.332(42)
11.0	4.65	4700	105.7185	2.493	0.088	16.39	0.303	0.71	0.34	350	400	2.851(42)

Y=0.25 Z=0.008

5.0	3.30	6000	4.7927	1.621	0.099	44.11	0.863	0.09	0.52	1050	1300	9.477(40)
-----	------	------	--------	-------	-------	-------	-------	------	------	------	------	-----------

TABLE 4—*Continued*

M^a	$\log L^b$	T_e^c	P^d	$\log \bar{R}^e$	$\Delta R/R_{ph}^f$	Δu^g	ΔM_{bol}^h	$\Delta \log g_s^i$	$\Delta \log g_e^j$	ΔT^k	ΔT_e^l	KE^m
(1)	(2)	(3)	(4)	(5)	(6)	(7)	(8)	(9)	(10)	(11)	(12)	(13)
5.0	3.30	5800	5.3695	1.651	0.114	53.75	0.801	0.10	0.59	900	1100	1.113(41)
5.0	3.30	5600	6.0578	1.680	0.098	44.37	0.534	0.09	0.50	600	750	1.150(41)
5.0	3.30	5400	6.8315	1.708	0.070	31.40	0.318	0.06	0.35	400	500	4.960(40)
5.0	3.30	5300	7.2680	1.722	0.045	18.30	0.186	0.04	0.21	250	300	1.454(40)
7.0	3.85	5700	13.6624	1.940	0.053	17.38	0.330	0.05	0.21	400	500	5.632(40)
7.0	3.85	5600	14.6120	1.959	0.137	47.55	0.918	0.11	0.62	1150	1400	3.535(41)
7.0	3.85	5500	15.6416	1.978	0.186	63.19	1.247	0.16	0.93	1550	1900	7.375(41)
7.0	3.85	5400	16.7248	1.996	0.218	72.31	1.377	0.19	1.10	1650	2050	1.093(42)
7.0	3.85	5300	17.8802	2.013	0.232	75.29	1.220	0.20	1.03	1450	1800	8.339(41)
7.0	3.85	5200	19.0636	2.028	0.231	71.04	1.024	0.20	1.00	1250	1550	6.341(41)
7.0	3.85	5100	20.3106	2.041	0.213	61.46	0.902	0.19	0.91	1150	1400	4.341(41)
7.0	3.85	5000	21.6381	2.055	0.199	52.97	0.778	0.17	0.84	1000	1250	3.138(41)
7.0	3.85	4900	23.1643	2.070	0.187	46.63	0.645	0.16	0.76	850	1050	2.893(41)
7.0	3.85	4800	24.7424	2.084	0.172	41.49	0.507	0.15	0.65	700	850	3.214(41)
7.0	3.85	4700	26.4054	2.096	0.123	29.12	0.318	0.11	0.42	450	550	1.816(41)
9.0	4.25	5300	34.3272	2.208	0.185	46.63	0.889	0.17	0.72	1000	1250	1.388(42)
9.0	4.25	5200	36.8545	2.228	0.223	50.56	1.036	0.21	0.86	1150	1400	1.847(42)
9.0	4.25	5100	39.4494	2.244	0.234	52.87	1.030	0.25	0.86	1100	1350	1.969(42)
9.0	4.25	5000	42.1071	2.260	0.233	52.98	0.972	0.28	0.85	950	1200	2.054(42)
9.0	4.25	4900	45.1198	2.274	0.223	49.96	0.831	0.31	0.80	850	1050	2.011(42)
9.0	4.25	4800	48.2842	2.289	0.188	46.00	0.664	0.33	0.74	750	950	1.736(42)
9.0	4.25	4700	51.6869	2.304	0.194	42.01	0.653	0.36	0.68	700	850	1.487(42)
9.0	4.25	4600	55.3677	2.318	0.177	37.66	0.585	0.38	0.60	600	750	1.211(42)
9.0	4.25	4500	59.2946	2.332	0.156	32.64	0.503	0.40	0.52	500	650	9.138(41)
9.0	4.25	4400	63.4315	2.346	0.132	26.76	0.406	0.42	0.42	400	500	6.104(41)
9.0	4.25	4300	67.6799	2.358	0.101	19.76	0.288	0.44	0.31	300	400	3.128(41)
9.0	4.25	4200	71.6850	2.368	0.006	10.56	0.135	0.44	0.16	150	200	8.980(40)
11.0	4.65	5200	75.0710	2.418	0.022	4.35	0.094	0.53	0.07	100	150	5.107(40)
11.0	4.65	5100	80.4266	2.435	0.084	15.03	0.319	0.59	0.23	400	450	2.205(41)
11.0	4.65	5000	86.3803	2.453	0.113	20.53	0.446	0.63	0.34	500	600	5.499(41)
11.0	4.65	4900	92.6797	2.469	0.125	22.85	0.498	0.67	0.38	500	650	9.420(41)
11.0	4.65	4800	100.2516	2.484	0.107	18.72	0.370	0.69	0.32	400	500	1.257(42)
11.0	4.65	4650	112.1748	2.507	0.099	16.43	0.330	0.74	0.32	350	400	2.226(42)
11.0	4.65	4600	116.7736	2.515	0.092	14.75	0.315	0.76	0.30	300	350	1.676(42)

Y=0.28 Z=0.02

5.0	3.30	5700	5.8631	1.664	0.054	22.65	0.364	0.05	0.23	450	550	4.435(39)
5.0	3.30	5600	6.2267	1.679	0.065	27.93	0.414	0.06	0.30	500	600	9.396(39)
5.0	3.30	5500	6.6094	1.695	0.066	27.66	0.369	0.06	0.32	450	550	3.774(40)
5.0	3.30	5400	7.0148	1.709	0.055	21.65	0.258	0.05	0.27	300	400	3.340(40)
7.0	3.85	5200	19.5354	2.024	0.162	43.76	0.749	0.14	0.61	900	1150	2.467(41)
7.0	3.85	5100	20.9006	2.042	0.187	48.62	0.771	0.16	0.72	950	1150	2.705(41)
7.0	3.85	5000	22.3729	2.059	0.200	49.96	0.735	0.17	0.77	900	1100	2.968(41)
7.0	3.85	4900	23.9614	2.076	0.206	49.68	0.694	0.18	0.78	850	1050	3.432(41)
7.0	3.85	4800	25.5723	2.093	0.208	48.64	0.675	0.18	0.77	800	1000	3.539(41)
7.0	3.85	4700	27.5304	2.109	0.203	46.59	0.632	0.18	0.72	750	950	3.950(41)

TABLE 4—*Continued*

M^a	$\log L^b$	T_e^c	P^d	$\log \bar{R}^e$	$\Delta R/R_{ph}^f$	Δu^g	ΔM_{bol}^h	$\Delta \log g_s^i$	$\Delta \log g_e^j$	ΔT^k	ΔT_e^l	KE^m
(1)	(2)	(3)	(4)	(5)	(6)	(7)	(8)	(9)	(10)	(11)	(12)	(13)
7.0	3.85	4600	29.5150	2.125	0.191	43.20	0.583	0.17	0.66	700	850	3.981(41)
7.0	3.85	4500	31.6742	2.140	0.167	37.07	0.482	0.15	0.57	550	700	3.633(41)
7.0	3.85	4400	33.9948	2.153	0.121	26.16	0.304	0.11	0.38	350	450	1.903(41)
9.0	4.25	4900	46.6106	2.269	0.036	7.24	0.122	0.23	0.07	100	100	2.464(40)
9.0	4.25	4800	50.2708	2.292	0.173	34.56	0.662	0.33	0.54	650	850	7.656(41)
9.0	4.25	4700	53.9918	2.310	0.188	37.68	0.695	0.37	0.60	700	850	9.653(41)
9.0	4.25	4600	58.0595	2.327	0.191	38.20	0.688	0.40	0.61	650	800	1.072(42)
9.0	4.25	4500	62.3935	2.343	0.187	37.50	0.655	0.44	0.59	600	700	1.115(42)
9.0	4.25	4300	72.2404	2.375	0.161	31.47	0.533	0.49	0.49	500	600	9.806(41)
9.0	4.25	4100	83.2813	2.404	0.111	20.26	0.319	0.53	0.33	300	400	5.051(41)
9.0	4.25	3900	94.3210	2.425	0.035	5.82	0.082	0.55	0.09	100	100	7.618(40)
11.0	4.65	4800	105.6869	2.488	0.050	7.60	0.154	0.68	0.13	150	200	3.203(40)
11.0	4.65	4700	113.7407	2.505	0.055	8.19	0.151	0.71	0.13	150	200	2.815(40)
11.0	4.65	4600	122.4423	2.522	0.077	11.30	0.212	0.76	0.19	250	300	3.918(41)
11.0	4.65	4500	132.4339	2.539	0.082	11.55	0.253	0.80	0.23	250	300	7.658(41)

^a Stellar mass (solar units). ^b Logarithmic luminosity (solar units). ^c Effective temperature (K). ^d Period (day).
^e Logarithmic mean radius (solar units). ^f Fractional radius variation. ^g Radial velocity amplitude (Kms⁻¹).
^h Bolometric amplitude (mag). ⁱ Amplitude of logarithmic static gravity. ^j Amplitude of logarithmic effective gravity. ^k Surface temperature variation (K). ^l Effective temperature variation (K). ^m Total kinetic energy (erg).

TABLE 5

ANALYTICAL RELATIONS FOR THE EFFECTIVE TEMPERATURE OF FUNDAMENTAL EDGES AT FIXED CHEMICAL COMPOSITION. $\log T = \alpha + \beta \log L/L_\odot$

Z^a	α^b	β^c	σ^d	α^b	β^c	σ^d
		FBE ^e			FRE ^f	
0.004	3.905	-0.035	0.004	3.995	-0.080	0.008
	$\pm 0.004^g$	± 0.004		± 0.008	± 0.006	
0.008	3.919	-0.043	0.008	4.030	-0.094	0.008
	± 0.008	± 0.006		± 0.009	± 0.005	
0.02	3.959	-0.061	0.006	4.125	-0.124	0.011
	± 0.006	± 0.004		± 0.011	± 0.009	

^aMetal content. ^b Zero point. ^c Luminosity coefficient ^d Standard deviation. ^e Fundamental blue edge. ^f Fundamental red edge. ^g Errors on coefficients.

TABLE 6
 FUNDAMENTAL PULSATION RELATIONS AT FIXED CHEMICAL COMPOSITION.
 $\log P = \alpha + \beta \log T_e + \gamma \log M/M_\odot + \delta \log L/L_\odot$

Z^a	α^b	β^c	γ^d	δ^e	σ^f
0.004	10.971	-3.387	-0.813	0.929	0.008
	$\pm 0.008^g$	± 0.034	± 0.030	± 0.008	
0.008	10.557	-3.279	-0.795	0.931	0.008
	± 0.008	± 0.036	± 0.032	± 0.008	
0.02	9.874	-3.108	-0.767	0.942	0.008
	± 0.008	± 0.042	± 0.039	± 0.010	

^aMetal content. ^b Zero point. ^c Effective temperature coefficient. ^d Mass coefficient. ^e Luminosity coefficient. ^f Standard deviation. ^g Errors on coefficients.